NTNU
Norwegian University of
Science and Technology

A thermodynamic study of the hydrogen dissociation by the Small System Method and the reactive force field ReaxFF

Nora Meling Eriksen

Chemistry
Submission date: May 2016
Supervisor: Signe Kjelstrup, IKJ
Co-supervisor: Thuat Trinh, IKJ

Norwegian University of Science and Technology
Department of Chemistry

Acknowledgements

I would like to thank my supervisors; Signe Kjelstrup for accepting me as part of her research group and giving me the opportunity to work under her tutelage, Thuat T. Trinh for his patience, guidance and mean-square displacement code and Ragnhild Skorpa for lending me all her books. In addition, I would like to thank Bjørn Strøm for sharing his Small System Method code and helping me to implement it on my system, Jan Inge Meling for technical support and Ole-Bjørn Ellingsen Moe for support in general. Since this thesis is the result of five years of study at NTNU, I would also like to thank my classmates for going on this journey with me and for taking many coffee breaks.

Lastly, I would also like to thank the entire non-equilibrium thermodynamics research group for listening to my presentations and for giving my feedback.

Abstract

The aim of this thesis was to study the reaction $2H=H_2$ using the reactive interaction potential ReaxFF. This was done by performing a thermodynamic study, using the ReaxFF and the Small System Method (SSM). The results were compared with several of the thermodynamic parameters from the article *The reaction enthalpy of hydrogen dissociation calculated with the Small System Method from simulation of molecular fluctuations* written by Skorpa *et al.* (2014) who used the reactive three-body potential (TBP). The ReaxFF was chosen because it is a popular interaction potential that is applicable with several chemical reactions and has low computational cost. An additional aim was conclude whether or not it was feasible to use the ReaxFF instead of the TBP and still get reasonable results.

In short, the ReaxFF produced fast calculations, which were consistent with expected trends. Here, the self-diffusion coefficient for H was larger than for H_2, whereas the heat capacity for H_2 was larger than for H. Furthermore, the activation energy was equal to the average bond enthalpy for hydrogen. By comparing the dissociation, partial molar enthalpy and the thermodynamic correction factor with the values in the Skorpa *et al.* paper, it was concluded that the ReaxFF compares to the TBP. Here, the ReaxFF and the TBP values were equal, or close to equal. In general, the ReaxFF values had higher uncertainties and deviated more from the TBP when the particle number was low. This was expected since the ReaxFF is a less accurate potential, however, it was argued that it could also be an effect of the post-modelling processing.

During testing an error in the SSM code in LAMMPS was discovered; the code could not recognize molecules. Consequently, it could not be used in this study. This resulted in more post modelling calculations than expected, leading to a second SSM code in MATLAB being used in order to obtain the thermodynamic correction factor.

To conclude, the ReaxFF simulates hydrogen dissociation as expected. Furthermore, it is feasible to use the ReaxFF instead of the TBP. Despite the TBP being a more accurate potential, the ReaxFF produces close to the same values, is more applicable and faster.

Sammendrag

Hensikten med denne oppgaven var å studere reaksjonen $2H=H_2$ ved å bruke det reaktive interaksjonspotensialt ReaxFF. Dette ble gjort ved å utføre en termodynamisk undersøkelse med ReaxFF og en nyutviklet *Small System Method* (SSM) kode i LAMMPS. Resultatene ble sammenlignet med samtlige termodynamiske parametere fra artikkelen *The reaction enthalpy of hydrogen dissociation calculated with the Small System Method from simulation of molecular fluctuations* skrevet av Skorpa *et al.* (2014) hvor interaksjonspotensialt *three-body potential* (TBP) ble brukt. ReaxFF ble valgt fordi det er et populært interaksjonspotensialt med lav beregningskostnad, som òg kan brukes til å simulere andre reaksjoner. En ytterligere hensikt var å konkludere hvorvidt det er mulig å bruke ReaxFF istedenfor TBP og fortsatt få rimelige resultater.

Kort oppsummert, ReaxFF produserte raske beregninger som var i samsvar med forventede trender og verdier. Her var selv-diffusjons koeffisienten for H større enn for H_2 og varmekapasiteten for H_2 var større enn for H. Videre var aktiveringsenergien lik den gjennomsnittlige bindingsentalpien til hydrogen. Sammenlignet med TBP produserte ReaxFF tilnærmet like verdier, men produserte generelt verdier med høyere unøyaktighet, samt avviket mer fra TBP når antallet partikler var lavt. Dette var ventet siden ReaxFF er et mindre nøyaktig potensial. Det ble hevdet at denne unøyaktigheten også kunne være en effekt av etter-modellerings behandlingen.

Under testing ble en feil i SSM koden oppdaget; molekylene ble ikke gjenkjent. Dermed ble den ikke brukt i oppgaven. Dette resulterte i flere etter-modelleringsberegninger enn forventet, hvor en ny SSM kode i MATLAB ble benyttet for å oppnå den termodynamiske korreksjonsfaktoren.

Det ble konkludert at ReaxFF simulerte hydrogen-dissosiasjon som forventet. Det er altså mulig å bruke ReaxFF istedenfor TBP. Til tross for at TBP er et mer nøyaktig potensial, produserte ReaxFF nær de samme verdiene, er mer anvendelig og raskere

.

Contents

Acknowledgements .... **iii**

Abstract .... **v**

Sammendrag .... **vii**

Contents .... **ix**

1. Introduction **1**

1.1. Scope 2

1.2. The structure of the thesis 2

2. Theory **3**

2.1. Diffusion 3

2.2. Activation energy 4

2.3. Enthalpy 5

2.4. The thermodynamic correction factor 7

2.5. Ensembles 7

3. Method **9**

3.1. Molecular dynamics simulation 9

3.1.1. Errors related to molecular dynamic simulation 10

3.1.2. Effects on the diffusion coefficient 11

3.2. Interaction potential 11

3.2.1. Classical force field 11

3.2.2. ReaxFF 12

3.2.3. Three body potential 14

3.3. Small System Method 15

3.3.1. Calculation of parameters with the Small System Method 16

4. Simulation details **19**

4.1. The system 19

4.2. Procedure 20

4.2.1. Non-reactive classical force field 20
4.2.2. Reactive ReaxFF 21
4.3. Interaction parameters 22
5. Results and discussion 25
5.1. Non-reactive classical force field 25
5.1.1. Pressure 26
5.1.2. Diffusion 28
5.1.3. Heat capacity 29
5.1.4. Thermodynamic correction factor 32
5.2. Reactive ReaxFF 33
5.2.1. Diffusion 34
5.2.2. Heat capacity 36
5.2.3. The thermodynamic correction factor 38
5.2.4. Heat of reaction, equilibrium constant 41
5.3. A review of the data processing and simulation parameters 45
6. Conclusion and outlook 47
References 49

Appendix A: Calculations of the theoretical self-diffusion coefficients

Appendix B: Uncertainty propagation

Appendix C: Overview of the state variables used in the simulations

Appendix D: MATLAB codes

Appendix E: ReaxFF input in LAMMPS

Symbol List

Table of Figures

Table of Tables

1. Introduction

Computer simulations are an expanding tool and are often preferred over experimental methods when it is too difficult, expensive or dangerous to perform an experiment. Moreover, using computer simulations provide unique atomistic insight into the behavior of the substance of interest. Potential-based methods (e.g. molecular dynamics) are computational tools that use interaction potentials. An interaction potential is a mathematical description of molecules and atoms behavior, alone and with others. They are parametrized to fit either experimental or quantum mechanical results[1]. Choosing the right interaction potential can be crucial when it comes to accuracy and computational costs. One of these interaction potentials is the ReaxFF developed by van Duin *et al.* (2001)[2]. This is a bond-order-dependent potential with van der Waals and Coulomb forces which is used to simulate the breaking and forming of bonds. Several applications using ReaxFF have been reported; dissociation of H_2 on platinum surfaces[3], thermal decomposition of polymers[4] and organic reactions[2] to name a few. [5]

A central problem in the chemical industry is to understand and operate chemical reactors. Here, chemical reactions take place under gradients such as concentration and temperature. It is important to get information about the transport properties of reactants and products and the enthalpy of reaction as a function of composition and temperature. In her dr. thesis Skorpa studied both enthalpy- and transport properties of a simple hydrogen dissociation in gas phase, using molecular dynamics simulations. This study was performed to facilitate the modelling of the coupled transport phenomena that occurs in a water gas shift reactions where a palladium membrane is used. Here, she used a three-body interaction potential. [6, 7]. This potential is more accurate but comes with a higher computational cost compared with ReaxFF. Furthermore, Skorpa studied only one reaction. This thesis aims to expand on her results by studying other more realistic chemical and surface reactions.

The first step to study more realistic reactions is to study the ReaxFF, which is applicable with many chemical reactions. A central part in performing this study is using a newly developed code for the Small System Method (SSM) in LAMMPS. The SSM uses fluctuation data from small systems and appropriate scaling to find thermodynamic limit values, making it possible to compare nano-scale systems with macro systems.[8] The combination of SSM and the ReaxFF will be a new way to obtain data for chemical reactors, and will be of high interest for both the chemical and chemical engineering community. The SSM has until today been used to successfully find activity coefficients and enthalpies for mixtures and electrolytes[9], CO_2 adsorption on surface [10] and the reaction enthalpy of $2H=H_2$[7].

1.1. Scope

The aim of this thesis is to study, as an example, the reaction $2H=H_2$ using the ReaxFF. This is done by performing a thermodynamic study, using the ReaxFF and the SSM. The results are compared with several of the thermodynamic parameters from the article *The reaction enthalpy of hydrogen dissociation calculated with the Small System Method from simulation of molecular fluctuations* written by Skorpa *et al.* (2014)[7]. Here, the simulation package LAMMPS[11] is used to perform the molecular dynamic simulations. By the end of this study it should be possible to conclude if it is feasible to use the ReaxFF instead of the three-body potential and still get reasonable results.

Even though the main purpose is to study the ReaxFF and compare the values with the three-body interaction potential, an additional non-reactive interaction potential, the classical force field, is also implemented. Its purpose is to test the system before implementing the ReaxFF. The results are compared with experimental and theoretical values to see if the values are reasonable. Additional testing is also performed on the system with the ReaxFF to see if it is implemented correctly.

1.2. The structure of the thesis

This thesis is divided into six main parts. First, a brief introduction into the thermodynamics and mathematical concepts used in this paper is presented in Chapter 2, and the methods used in the simulations follow in Chapter 3. Among these are the different interaction potentials of interest. In Chapter 4, the simulation details are presented, followed by the results and discussion in Chapter 5. Lastly, the conclusion and outlook is presented in Chapter 7.

For the purpose of this thesis, “the method” refers to the interaction potential in combination with a simulation package. In this thesis, the interaction potentials ReaxFF and classical force field are used separately in combination with the simulation package LAMMPS. “The system” refers to a square box or sphere with hydrogen atoms and/or molecules.

2. Theory

The purpose of this section is to give a short theoretical background of the thermodynamics used in this thesis. The thermodynamics will include mathematical concepts which are presented chronologically as follows; mean square displacement, activation energy, enthalpy, the thermodynamic correction factor and the different ensembles used.

2.1. Diffusion

The random molecular motion that leads to the molecules spreading in a given medium is called diffusion. Fick's law (Equation(1)) describes this mass flux of one of the components in one dimension.

$$J_i = aj_i = -aD\frac{\partial c_i}{\partial z} \tag{1}$$

Here, J_i is the total flux, j_i is the flux per unit area, c_i is the concentration, z is the distance, a is the cross sectional area and D is the diffusion coefficient, which Fick called "the constant depending of the nature of the substances"[12, 13].

In the absence of a concentration gradient, the flux of one component is described by the self-diffusion coefficient. Einstein related the self-diffusion coefficient to the mean square displacement (MSD) of a particle as a function of time, t. As shown in Equation(2) is the self-diffusion coefficient, D_{self}, the proportionality constant that relates the MSD to the time, as the time goes to infinity[14]

$$D_{self} = \frac{1}{2d}\lim_{t\to\infty}\frac{\left\langle [r(t_0+t)-r(t_0)]^2 \right\rangle}{t} \tag{2}$$

Here, d is the dimensionality of the system and r is the molecule position. The numerator of Equation(2) is the MSD. The self-diffusion coefficient of a species can be obtained through linear least squares regression, as shown in Equation(3).[14].

$$\left\langle [r(t_0+t)-r(t_0)]^2 \right\rangle = b_0 + (2dD_{self})t \tag{3}$$

Here, b_0 is the intercept and $2dD_{self}$ is the slope. Even though it has been proven difficult to develop theories for a-priori calculations of the diffusion coefficient and perform experimental measurements, the gaseous diffusion coefficient can be estimated theoretically.

These values are often estimated to lie between 0.1 and 1 cm^2/sec at 1atm and near room temperature.[12]

The Chapman-Enskog theory (aka. kinetic gas theory) for gaseous diffusion coefficients is based on the detailed analysis of molecular motion in dilute gases. The equation for two components is shown in Equation(4). This theory is accurate to an average of 8% and is based on the assumption of nonpolar gases[12].

$$D = \frac{1.86 \cdot 10^{-3} T^{3/2} (1/\tilde{M}_1 + 1/\tilde{M}_2)^{1/2}}{p \sigma_{12}^2 \Omega} \tag{4}$$

Here, T is the temperature, p is the pressure, $\tilde{M}_i$ are the molecular weights, σ_{12} is the collision diameter (the closest distance between two colliding atoms) which is the average of the two species present, as shown in Equation(5), and Ω is a dimensionless quantity which is dependent on the integration of the interaction (e.g. Lennard-Jones 12-6 potential) between the two components. The latter resulting in an integral that varies with the interaction energy and temperature. This energy, ε_{12}, is a geometric average of contribution from the two species, as shown in Equation(6).

$$\sigma_{12} = \frac{1}{2}(\sigma_1 + \sigma_2) \tag{5}$$

$$\varepsilon_{12} = \sqrt{\varepsilon_1 \varepsilon_2} \tag{6}$$

Ω and σ_{12} are molecular properties characteristic for the detailed theory and can be found in literature[12]. When calculating D_{self} using kinetic gas theory is a simplified version of Equation (4) used (see Attachment A).

2.2. Activation energy

The activation energy, E_a, is in some ways a barrier to energy transfer over which the reacting particles must exceed to go from kinetic- to potential energy. [15] Since the activation energy of hydrogen dissociation is the energy equivalent to breaking a hydrogen bond, it can be compared with the average bond enthalpy for H_2, ΔH_f. The activation energy can be found using Arrhenius plot, as shown in Equation(7).

$$\ln k_r = \ln A - \frac{E_a}{RT} \tag{7}$$

Here, k_r is the rate constant, A is called the pre-exponential factor or the ‘frequency factor’ and R is the universal gas constant. A plot of $\ln k_r$ against $1/T$ gives a straight line, where $(-E_a/R)$ is the slope. The graph’s shape is a result of the particles kinetic energy, which increases with temperature, thus increasing the reaction rate. Consequently, in this instance, the bonds are more susceptible to be broken. k_r is a rate expressed as a change in concentration, $[A]$, divided by t. For a first order reaction k_r can be found as shown in Equation(8), which produces a plot that also gives a straight line. If the plot do not have a straight line, it indicates that the reaction has another order.[16]

$$-\mathrm{k} = \frac{\partial \ln[\mathrm{A}]}{\partial \mathrm{t}} \tag{8}$$

2.3. Enthalpy

Enthalpy, H, is a state function that gives information about the amount of heat exchanged between the system and its surroundings and is defined in as shown in Equation(9).

$$\mathrm{H} \equiv \mathrm{U} + \mathrm{pV} \tag{9}$$

Here, U is the internal energy and the pV is the pressure-volume work that is done by the system on the surroundings. In a process, heat capacity, C, is used to calculate the change in H. It is defined as the amount of heat required, q, to increase the temperature of a given matter by 1 K. The heat capacity at constant p is defined as shown in Equation(10).[17]

$$\mathrm{C_p} = \left(\frac{\mathrm{dq}}{\mathrm{dT}}\right)_{\mathrm{p}} \equiv \left(\frac{\mathrm{dH}}{\mathrm{dT}}\right)_{\mathrm{p}} \tag{10}$$

In other words, the heat capacity is a matter’s ability to absorb heat, which is dependent on the molecule’s kinetic energy, i.e. the shape and movement of molecules. There are three ways which a molecule can move; vibration, translation and rotation. The molecular movement is shape dependent. In Figure 2.1 are the movements possible for a hydrogen molecule and atom illustrated. As shown, the molecule has three ways to move, whereas the atom only has one, resulting in a greater heat capacity for hydrogen molecules compared with hydrogen atoms.[17]

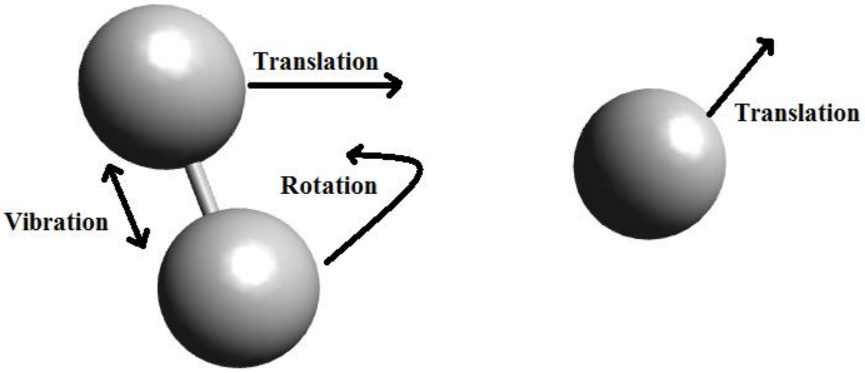

Figure 2.1: The movements for hydrogen molecule and atom. As shown, the molecule has three different movements whereas the atoms only as one.

The partial molar enthalpy is an intensive variable that describes the change in enthalpy as the number of moles for a given species changes while all other variables are kept constant. Equation(11) show the partial molar enthalpy for species *i*, $h_{i.}$ [17]

$$h_i = \left(\frac{\partial H}{\partial n_i} \right)_{T,P,n_k} \tag{11}$$

Here, *H* is the total enthalpy of the system and n_i is the number of moles of species *i*. The variables *T*, *p* and number of moles in the system that is not of species *i*, n_k, are kept constant. The molar heat capacity (heat capacity per mole) for species *i*, $C_{p,i}$, at constant *p* shown in Equation(12).[17]

$$C_{p,i} = \left(\frac{\partial h_i}{\partial T} \right)_p \tag{12}$$

For ideal gas is $C_{p,i}$ equal to 5/2R and 9/2R for monoatomic and diatomic gas, respectively. The standard reaction enthalpy, $\Delta_r H°$, is the change in enthalpy when one mole of a species is transformed during a chemical reaction under standard conditions. This parameter can be calculated with van’t Hoff equation at constant pressure, as shown in Equation(13).[17]

$$\left[\frac{d \ln K_{th}}{d(1/T)} \right] = -\frac{\Delta_r H°}{R} \tag{13}$$

The the dissociation constant, K_x, is a function of the mole fractions, X_i, for the components in a given system. The thermodynamic equilibrium constant, $K_{th,}$ is a function of K_x and the activity coefficients, γ_i. For a system with hydrogen atoms and molecules can K_{th} be found as shown in Equation(14).

$$\mathrm{K}_{\mathrm{th}} = \frac{\mathrm{X}_{\mathrm{H}}^{2}}{\mathrm{X}_{\mathrm{H}_2}} \frac{\gamma_{\mathrm{H}}^{2}}{\gamma_{\mathrm{H}_2}} = \mathrm{K}_{\mathrm{x}} \frac{\gamma_{\mathrm{H}}^{2}}{\gamma_{\mathrm{H}_2}} \tag{14}$$

For an ideal mixture $\gamma_H^2/\gamma_{\mathrm{H}_2}^2 = 1$ which result in $K_x = K_{th}$.[6]

2.4. The thermodynamic correction factor

The thermodynamic correction factor (TCF), Γ, is a measurement of non-ideality and is equal to one when the mixtures are ideal (the pressure is low to moderate)[18] It is defined as shown in Equation(15).[13]

$$\Gamma_{\mathrm{i}} \equiv \mathrm{N}_{\mathrm{i}} \left(\frac{\partial \mu_{\mathrm{i}}}{\partial \mathrm{N}_{\mathrm{i}}} \right)_{\mathrm{V,T,\mu_i}} \tag{15}$$

Here, μ_i is the chemical potential and N_i is number of particles of species *i*. The TCF relates the Fick diffusivity, *D*, and the Maxwell-Stefan diffusivity, *Đ*, as seen in Equation(16). [18]

$$\mathrm{D} = \text{Đ}\Gamma \tag{16}$$

2.5. Ensembles

Two ensembles are of interest in this thesis. The first is the canonical ensemble where N_i,V and T are constant. This ensemble is used when performing molecular dynamics simulations. This ensemble represents a closed system immersed in a very large heat bath. [19]

The second is the grand canonical ensemble is where μ_j,V and T are constant. This ensemble is used when using the Small System Method. This ensemble represents an open system immersed in a very large heat bath. Both heat and matter can enter and exit the system's walls.[19]

In their paper, Skorpa *et al.*[7] compared the partial molar enthalpy at the thermodynamic limit calculated with different densities and ensembles (μ_j,V,T), (N_j,V,T) and (N_j,P,T) for H and H_2. They found out that at the lowest density, $\rho=5.22$ kg/m^3, the difference was small, and at the lowest temperatures, $T\leq7799$K, the values for (μ_j,V,T) and (N_j,V,T) were equal for both particles. They concluded that the mixture is ideal under these conditions.[7]

3. Method

This chapter focuses on the different computational methods used in this thesis. First, the molecular dynamic simulation is described. Here, the focus is on the mathematical concepts behind this method, errors that can occur and effects its approximations have on the diffusion. Secondly, the different interaction potentials used in combination with the molecular dynamics are presented. Here, the basic principles behind the interaction potentials are explained. Lastly, the Small System Method, used to find the TCF and partial molar enthalpy, is presented.

3.1. Molecular dynamics simulation

Molecular dynamic (MD) simulation is a molecular modelling method that calculates the 'real' dynamics of a system to gain atomistic insight. This is done by constructing a macroscopic system and predicting its properties[20]. MD simulation follows the evolution of time where it can calculate any state from its current one, making it a deterministic method.[1, 20]. Here, MD simulation treat the N particles, that the system is comprised of, as point masses and integrates Newton's equations to gain their motions.[21] In LAMMPS is the *Verlet method* applied for the integrations[22]. Newton's law of motion is found in Equation(17).

$$\mathrm{m_i}\ddot{\mathbf{r}}_\mathrm{i} = \mathbf{f}_\mathrm{i} \tag{17}$$

Here, m_i is the mass of the particle i, $\ddot{\boldsymbol{r}}_\mathrm{i}$ is the second derivative of the position of the particle, in Cartesian coordinates, moving along with the force $\boldsymbol{f}_i$ [23]. The force is shown in Equation (18)

$$\boldsymbol{f}_i = \sum_\mathrm{j} \mathrm{F}_2(\boldsymbol{r}_\mathrm{i}, \boldsymbol{r}_\mathrm{j}) + \sum_\mathrm{j}\sum_\mathrm{k} \mathrm{F}_3(\boldsymbol{r}_\mathrm{i}, \boldsymbol{r}_\mathrm{j}, \boldsymbol{r}_\mathrm{k}) + \ldots \tag{18}$$

Here, F_2 and F_3 are force functions for the pair-wise and a three-body interaction. Additional many-body interactions can be added.[21] The first derivative of the position, $\dot{\boldsymbol{r}}_\mathrm{i}$, is a function the momentum, $\boldsymbol{p}_\mathrm{i}$, as shown in Equation(19), which again is a function of the potential, V, (see Section 3.2) as shown in Equation(20).

$$\dot{\boldsymbol{r}}_\mathrm{i} = \frac{\partial \hat{\mathrm{H}}}{\partial \boldsymbol{p}_\mathrm{i}} = \frac{\boldsymbol{p}_\mathrm{i}}{\mathrm{m_i}} \tag{19}$$

$$\dot{\boldsymbol{p}}_i = -\frac{\partial \hat{H}}{\partial \boldsymbol{r}_i} = -\frac{\partial V}{\partial \boldsymbol{r}_i} = \boldsymbol{f}_i \tag{20}$$

Both equations are derived using the classical Hamiltonian, $\hat{H}$. $\hat{H}$ is a function of 6N-3 dimensional phase space and can be written as a sum of kinetic and potential energy terms, as shown in Equation(21). [23]

$$\hat{H}(\boldsymbol{p}_i, \boldsymbol{r}_i) = \sum_{i=1}^{N} \frac{1}{2m_i} \boldsymbol{p}_i^2 + V(\boldsymbol{r}_i) \tag{21}$$

By gaining information about the motion of the particles in a system, it is possible to calculate useful micro- and macroscopic information.[21] Equation(22) shows how the momenta and positions can be used to calculate thermodynamic properties, *B*, such as pressure and heat capacity. Numerical integrating is used to calculate thermodynamic averages as time averages. Here M is the number of time steps.[20]

$$\langle B \rangle = \frac{1}{M} \sum_{i=1}^{M} B(\boldsymbol{p}^N, \boldsymbol{r}^N) \tag{22}$$

3.1.1. Errors related to molecular dynamic simulation

The errors related to the MD calculations are often similar to errors that can occur when preforming real experiments [24]. According to Frenkel and Smit the following errors are; *"(...) the sample is not prepared correctly, the measurement is too short, the system undergoes an irreversible change during the experiment, or we do not measure what we think."* [Frenkel and Smit, 2001, p.64,[24]]Even though molecular dynamics simulation tend to deliver accurate descriptions of systems, there are many effects that have been omitted, which can be crucial in certain cases[23]. According to Field in regards to the effects that have been omitted and examples of what these effects might lead to:

> (…) they may fail in the treatment of the dynamics of light particles (especially hydrogen), for which quantum mechanical tunneling effects can be important and they do not include zero-point motion, which is the vibrational motion that all quantum mechanical system undergo even at the absolute zero of temperature.
>
> [Field 2007, p.171,[23]]

Furthermore, the duration of the measurements is a consequence of the size and number of time steps. When choosing the time steps there are no hard rules to follow on how to get the optimum number, but choosing wrong can also lead to errors. Too small can give an unrepresentative trajectory of the phase space and too large can lead to high energy overlaps between atoms which may result in instabilities in the integration algorithm.[20]

3.1.2. Effects on the diffusion coefficient

In MD simulations, at constant *NVT*, is the Nosé-Hoover Thermostat used to reproduce a behavior for a system. This paper is not going to go into details about this thermostat, only mention that the Nosé-Hoover coupling constant *Q* affect the diffusion coefficient, resulting in a slight slope near origin in a MSD as a function of the observed time plot [24].

3.2. Interaction potential

Force field is a type of interaction potential used by molecular mechanics to study molecular conformations and largely determines the systems properties and behavior[23]. The equation for the interaction potential, $V(\boldsymbol{r}^N)$, consist usually of four components, which illustrates the intra- and intermolecular forces in the system, as shown in Equation(23).[20]

$$V(\boldsymbol{r}^N) = \text{bonds} + \text{angles} + \text{torsion} + \text{nonbonding} \tag{23}$$

The terms represent the energetic penalties that are given when deviation from equilibrium or reference state occur. The last term describe the non-bonding interactions. Additional terms can be added[20]. In this thesis, hydrogen is the only component used, thus only bond- and nonbonding contributions are taken into account when creating the different force fields. There are three interaction potential used in this thesis; the non-reactive classical force field, the reactive ReaxFF and the reactive classical three-body potential.

3.2.1. Classical force field

The non-reactive classical force field (denoted in this thesis as FF) is a combination of three potentials that has been tested previously by Simon *et al.* (2010) [25]. The first is the Morse potential that models the intramolecular interaction.

$$V(r)_M = D_e\left(1 - e^{-a(r-r_0)}\right) \tag{24}$$

Here, $a = \omega\sqrt{\mu / 2D_e}$ and $\omega = \sqrt{k / \mu}$, where the stretching bond constant, k, is divided by the reduced mass, μ, D_e is the depth of the potential energy minimum and r is the displacement from the reference bond length, r_0. The last to contributions make up the he non-bonding term.

$$V_{ij}^{nb} = V_{ij}^{LJ} + V_{ij}^{coulombic} \tag{25}$$

$$V_{ij}(r_{ij}) = 4\varepsilon_{ij}\left[\left(\frac{\sigma_{ij}}{r_{ij}}\right)^{12} - \left(\frac{\sigma_{ij}}{r_{ij}}\right)^{6}\right] \tag{26}$$

$$V_{ij}^{LJ}(r_{ij}) = \begin{cases} V_{ij}(r_{ij}) - V_{ij}(r_c) & \text{if } r_{ij} < r_c \\ 0 & \text{if } r_{ij} > r_c \end{cases} \tag{27}$$

The first contribution is a shifted and truncated Lennard- Jones (LJ) 12-6 potential that is used to model the van der Waals interactions. This function consists of the collision diameter, σ, the minimal potential between the particles, ε_{ij}, and the distance r_{ij} = |$\mathbf{r}_i$-$\mathbf{r}_j$|. The r^{-6} represents the repulsive part and r^{-12} the attractive[20]. The cut-off distance r_c, is the distance where the interaction between the molecules are zero, as shown in Equation(27).[26] The second contribution is the Coulomb potential that is used to model the electrostatic interactions between two particles *i* and *j*,

$$V_{ij}^{coulombic}(r_{ij}) = \frac{q_i q_j}{4\pi\varepsilon_0 r_{ij}} \tag{28}$$

The Coulomb potential consists of pairs of electric charge, q_i and q_j, with distance r_{ij} and the electrical permittivity of space, ε_0. The FF for H consist of a non-bonding term, only.[20]

The drawback related to the Morse potential is that it increases the simulation time by needing to specify three parameters for each bond.[20]

3.2.2. ReaxFF

The reactive force field ReaxFF was developed by van Duin *et al.* (2001) [2]. It is defined as a classical interaction potential that is bond-order-dependent. When modelling the breaking and forming of bonds, the bond-order, BO'_{ij}, is updated at every MD step. This is done by calculating the interatomic distance, *r(ij)* at each step.

$$BO'_{ij}(r_{ij}) = \exp\left[p_{bo,1} \cdot \left(\frac{r_{ij}}{r_0}\right)^{p_{bo,2}}\right] \tag{29}$$

Here, is r_0 the interatomic distance at equilibrium and can be calculated between atoms *i* and *j* as shown in Equation(30).

$$\mathrm{r_0(ij)} = \frac{1}{2}(\mathrm{r_0(i)} + \mathrm{r_0(j)}) \tag{30}$$

The bonding interaction is used to determine the connectivity. The sigma bond ($\mathrm{p_{bo,1}}$ and $\mathrm{p_{bo,2}}$) between to atoms is generally below ~1.5 Å and is negligible above ~2.5Å. Equation(29) has been simplified for this system since the maximum bond-order is 1 for a 2H=H_2 system. The BO'_{ij} is corrected by multiplying it with the correction factors f_4 and f_5 as seen in Equation(31) , creating a corrected bond order BO_{ij} .[2, 5]

$$\mathrm{BO}_{ij} = \mathrm{BO}'_{ij} \bullet f_4(\Delta'_i, \mathrm{BO}'_{ij}) \bullet f_5(\Delta'_i, \mathrm{BO}'_{ij}) \tag{31}$$

Here, Δ'_i is defined as "*the degree of deviation of the sum of the uncorrected bond orders around an atomic center form its valency*"[van Duin *et al.*, 2001, p.9398 [2]]. For H, the valency is 1. The bond interaction is obtained from the corrected bond order as shown in Equation(32). Here, $p_{be,1}$ and $p_{be,2}$ are bond parameters and D_e is the depth of the potential energy minimum.[2]

$$\mathrm{V^{Bond}}(\mathrm{r}_{ij}) = -D_e \bullet \mathrm{BO}_{ij} \bullet \exp\left[p_{be,1}(1 - \mathrm{BO}_{ij}^{p_{be,1}}) \right] \tag{32}$$

The non-bonded interaction is calculated between every atom pair and consists of the van der Waals forces and electrostatic interactions, which are independent of the connectivity. The van der Waals is modeled using a distance-corrected Morse potential (Equation(33)) which includes a shielding term, f_{13}, to avoid excessive close-range interactions, [5] thus making the non-bonded interactions become constant as $\mathrm{r_{ij}} \to 0$ [2].

$$\mathrm{V^{vdWaals}} = \mathrm{D}_{ij} \left(\mathrm{e}^{\alpha_{\mathrm{ij}} \bullet \left(1 - \frac{f_{13}(r_{ij})}{r_{\mathrm{vdW}}} \right)} - 2\mathrm{e}^{\frac{1}{2}\alpha_{\mathrm{ij}} \bullet \left(1 - \frac{f_{13}(r_{ij})}{r_{\mathrm{vdW}}} \right)} \right) \tag{33}$$

Here, D_{ij}, α_{ij} and r_{vdW} are van der Waals parameters. The Coulomb interaction is used to model the electrostatic interactions as shown in Equation(34). A shielded version with constant is used to adjust for orbital overlap at close distances.[2]

$$\mathrm{V^{Coulomb}} = \mathrm{C} \bullet \frac{q_i \bullet q_{\mathrm{j}}}{\left[\mathrm{r}_{ij}^3 + \left(1/\gamma_{ij} \right)^3 \right]^{1/3}} \tag{34}$$

Here, the potential is equal to the one used in the FF ($C=1/4\pi\varepsilon_0$), except for an additional shielded term γ_{ij}. [2]

A small time step is needed when using ReaxFF since charges and bond order change at every time step. On the contrary of what have been mentioned earlier have Chenoweth *et al.* (2008)[5] found out that to get the smooth reactions, collisions and an efficient coverage of the phase space at high temperatures (2500K),is 0.1 fs the optimal time step. A full description of the ReaxFF is found in van Duin *et al.*(2001)[2].

3.2.3. Three body potential

Skorpa *et al.* (2014)[7] used the interaction potential developed by Stillinger and Weber(1988)[27]. Here the interaction potential, *V*, consist of two - and three- particle interaction contributions ($v_{(2)}$ and $v_{(3)}$). In this thesis the potential is called the three-body potential (TBP).

$$V(\mathbf{r}_1,...,\mathbf{r}_N)=\sum_{i<j} v_{(2)}(r_{ij})+\sum_{i<j<k} v_{(3)}(\mathbf{r}_i,\mathbf{r}_j,\mathbf{r}_k) \tag{35}$$

The two- and three- particle interaction for hydrogen was derived by Kohen *et al.*(1998)[28], by using the quantum mechanical results of Diedrich and Anderson(1992,1994)[29, 30]. The two-particle interaction is shown in Equation(36), with the cut-off distance, r_c,

$$v_{(2)}(\mathbf{r})=\begin{cases} \alpha(\beta_2\mathbf{r}^{-p}\text{-}1)\exp\left[\dfrac{\gamma_2}{\mathbf{r}-\mathbf{r}_c}\right] & \text{if } r_{ij}< r_c \\ 0 & \text{if } r_{ij} > r_c \end{cases} \tag{36}$$

Here, α, β_2, γ_2 and *p* are constants. The constant α is added to get the minimum potential to result in the binding energy of hydrogen at the bond distance r_e = 0.74 Å. A bond is formed if the distance between to atoms is smaller than the cut-off distance, creating a molecule. Since a hydrogen atom can only have one bond, the three-particle interactions are added to prevent the formation of more. Thus, the potential is a sum of each particle contribution as shown in Equation(37).

$$v_{(3)}(\mathbf{r})=h_{i,j,k}(r_{ij},r_{jk},\theta_{i,j,k})+h_{j,i,k}(r_{ji},r_{ik},\theta_{j,i,k})+h_{i,k,j}(r_{ik},r_{kj},\theta_{i,k,j}) \tag{37}$$

Where the h-functions are given by

$$h_{j,i,k}(\mathrm{r}_{ji},\mathrm{r}_{ik},\theta_{j,i,k})=\begin{cases}\lambda a\, exp\left[\dfrac{\gamma_3}{(\mathrm{r}_{ji}-\mathrm{r}_\mathrm{c})}+\dfrac{\gamma_3}{(\mathrm{r}_{ik}-\mathrm{r}_\mathrm{c})}\right] & \text{if } \mathrm{r}_\mathrm{ij}< r_c \text{ and } \mathrm{r}_\mathrm{ik}< r_c \\ 0 & \text{otherwise}\end{cases} \tag{38}$$

And the *a* is

$$a=\left[1+\mu\cos(\theta_{j,i,k})+v\cos^2(\theta_{j,i,k})\right] \tag{39}$$

Here, λ, μ, v and γ_3 are constants. The middle letter in the triad subscript denotes the atom at the subtended angle vertex. Here, the distance is calculated in respect to this atom[7]. Weak van der Waals forces are established between two neighboring diatomic molecules when combining the two- and three particle potential[27]. A full description of the interaction potential for a hydrogen dissociation is found in Skorpa *et al.*(2014)[6].

3.3. Small System Method

The Small System Method (SSM) was developed by Schnell *et al.* [8], using Hill's thermodynamics for small systems[31]. The method was created to give a comparative basis between thermodynamic properties in macroscopic systems and in small systems. Thermodynamic properties from these two systems cannot be directly compared due the fact that enthalpy and Gibbs energy are not extensive (not proportional to the system size) in small systems. In addition, not much research has been provided in the field of nano-scale systems because of the difficulty level of preforming experiments. Here, the small systems are strongly influenced by surface effects. These effects are in principle, however, possible to simulate.[8]

The comparative basis is made possible by calculating thermodynamic properties form fluctuations in small non-periodic systems embedded in a periodic reservoir and scaling them. The scaling is performed by extrapolation of the thermodynamic properties as a function of the inverse system length in one dimension, *1/L*. By using the inverse length, the properties are found at the thermodynamic limit. In Figure 3.1, several sphere shaped small systems with varying radiuses are embedded in a cubic shaped reservoir.[8]

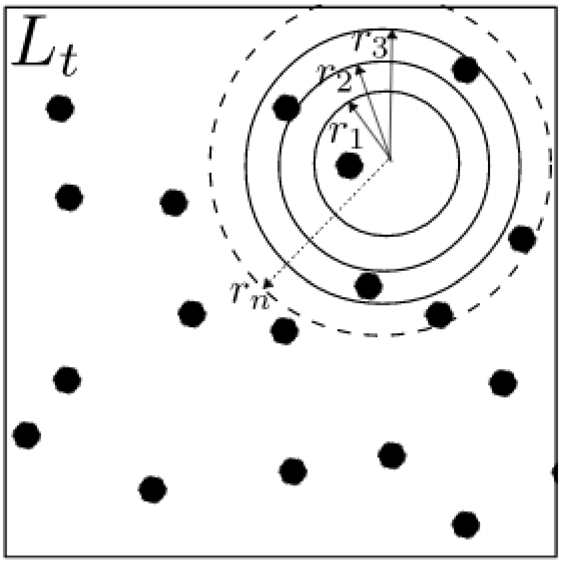

Figure 3.1: Illustration of the small systems embedded in a reservoir. Here, the reservoir with sides L_t is embedded with *n* small systems with varying radiuses (r_1,r_2…r_n). Macroscopic properties are obtained by calculating the thermodynamic properties in number of small systems randomly placed in the reservoir and scaling them through extrapolation of the inverse small system length. (Copyright Schnell *et al.* [32])

As shown, the reservoir has sides with length L_t and the *n* small systems have radiuses in varying sizes denoted as $r_1, r_2 \ldots r_n$. These small systems can exchange mass and energy with the reservoir. If the reservoir is simulated in the grand-canonical ensemble (see section 3.2), the small systems are too. If the reservoir has a different ensemble, the small systems are in the grand-canonical ensemble if $r_n << 0.5\ L_t$. The choice of reservoir ensemble in the thermodynamic limit is irrelevant.[8] To calculate the small system length, L_n, for each sphere, Equation(40) is used.

$$L_n = \left(\frac{4}{3}\pi\right)^{\frac{1}{3}} r_n \tag{40}$$

3.3.1. Calculation of parameters with the Small System Method

As mentioned, when using the SSM the thermodynamic properties are calculated from fluctuations in small non-periodic systems. Furthermore, the small system can exchange mass and energy with the reservoir. Consequently, the TCF and the partial molar enthalpy can be calculated from fluctuations of *N* and *U*. The TCF for a binary mixture with a grand-canonical ensemble is shown in Equation(41).

$$\Gamma_{ij}^{-1} = \frac{1}{\beta}\left(\frac{\partial \ln\langle N_i\rangle}{\partial \mu_j}\right)_{T,V,\mu_{k\neq i}} = \frac{\langle N_i N_j\rangle - \langle N_i\rangle\langle N_j\rangle}{\langle N_j\rangle} \tag{41}$$

Here, $\beta = k_B T$, where k_B is the Boltzmann constant. The TCF for only one component is shown in Equation(42).[8]

$$\Gamma_{ii}^{-1} = \frac{\langle N_i{}^2 \rangle - \langle N_i \rangle^2}{\langle N_i \rangle} \tag{42}$$

The partial molar enthalpy in a binary mixture with in a grand-canonical ensemble can be calculated with the SSM as shown in Equation(43).[33]

$$h_i = \left(\frac{\partial H}{\partial N_i} \right)_{T,V,\mu_{j \neq i}} = -\frac{\langle UN_i \rangle - \langle U \rangle \langle N_i \rangle + \langle N_i \rangle k_B T}{\langle N_i^2 \rangle - \langle N_i \rangle^2} \tag{43}$$

The TDC and partial molar enthalpy are linear functions of 1/*L*, as shown in Equation(44) and (45), respectively. Here, the thermodynamic properties can be found at the thermodynamic limit through extrapolation.[32]

$$\Gamma_{ii}^{-1}(L) = \Gamma_{ii,\infty}^{-1} + \frac{A_{ij}}{L} + \ldots \tag{44}$$

$$h_i^{-1}(L) = h_{i,\infty}^{-1} + \frac{A_i'}{L} + \ldots \tag{45}$$

4. Simulation details

In this chapter are details given on how different values of thermodynamic properties are obtained for systems with the reactive force field, ReaxFF, and the non-reactive force field, FF. First, the system in general is presented, followed by the procedure, which includes the simulation details and how the thermodynamic properties are calculated post modelling. Lastly, the interaction parameters for the interaction potentials are presented.

The volumes in this thesis are given as the side length cubed. This is because the system is a cubic box where all the sides are at equal length. It is more representative to state the side length then the volume since it is a smaller number, making the different sizes easier to compare quantitatively.

4.1. The system

The system was a cubic box with periodic boundary conditions (PBC) in x, y and z direction. The box size was varied in size from 28.47^3 to 100^3 Å^3, the number of particles in the system varied from 37 to 1500 and temperature varied from 100 to 20796 K. The reaction $2H=H_2$ was simulated using the MD simulator LAMMPS[11]. The simulations had 1,000,000 to 10,000,000 time steps that varied from 0.1 to 1 fs, printing the temperature, pressure, potential energy and MSD at every 500th time step and storing them for further analysis by LAMMPS using the “thermo_style” command. An additional output file containing the trajectories for each particle at each 500 time step was created using the “dump” command. The total amount of simulations performed in this thesis is 55, 49 using the FF and 6 using the ReaxFF. The number of simulations per system varied from 5 to 15.

All calculations were performed in a (N_j, V, T) ensemble, except when using the SSM, which uses a (μ_j, V, T) ensemble. The calculations were compared with ideal gas, experimental values and/or parameters calculated for the same system using the reactive TBP as interaction potential[7]

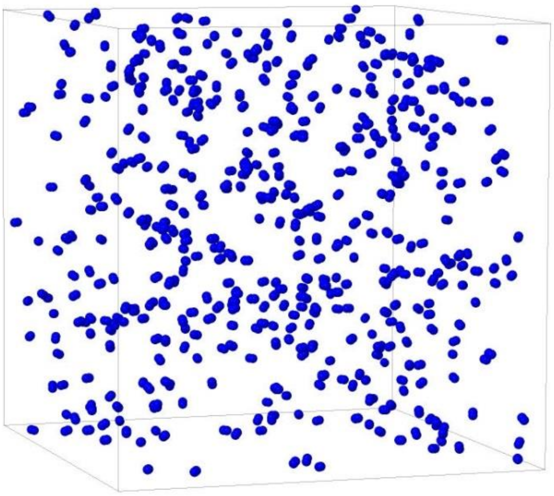

Figure 4.1: A snap shot of the system at density, ρ=1.67kg/m^3.

4.2. Procedure

The procedure is divided into two sections, depending on the interaction potential used. The first interaction potential is the non-reactive, FF. This force field is implemented in LAMMPS to test the hydrogen system by calculating different thermodynamic properties. These properties include; the pressure with varying state variables, the MSD, the partial molar enthalpy and the TCF. The two latter parameters are calculated to test the newly developed SSM code in LAMMPS.

The second interaction potential is the reactive ReaxFF. This force field is implemented on the same system as the FF. The only difference is that a reaction can now take place. With this new reactive force field, additional testing is performed. This is done by calculating the MSD and activation energy for ReaxFF. After the testing the thermodynamic parameters will be calculated under the same conditions as in Skorpa *et al.* [7]. The results will be compared to the results the TBP produced. These parameters include; the partial molar enthalpy, the TCF and the reaction enthalpy.

4.2.1. Non-reactive classical force field

First, the system was tested by calculating the pressure at different conditions, e.g. different temperatures (100-300K), number of molecules (250-1500) and mole fractions of H_2 (0-1). The box size was kept constant at 100^3 Å^3. When the variables were not varied they were fixed at 1000 molecules and either at 100, 300 or 500K. The results were compared with experimental values[34] and/or ideal gas behavior.

Since the topology is known when using non-reactive force fields (which atoms make a molecule), the MSD was calculated using a built-in function in LAMMPS. Here, the system was tested by calculating the MSD at different mole fractions of H_2 at 300K with constant number of particles N_{tot}=1000 ($N_{tot}=N_{H_2}+N_H$). The self-diffusion coefficient was obtained and compared with kinetic gas theory (Chapman-Enskog theory)

In the last test the newly developed SSM code in LAMMPS was used. Here, 30 sub volumes (spheres) with a radius ranging from $0.05L_t$ to $0.5L_t$ were randomly sampled 30 times in the system at every 500 time steps. First, SSM code was tested with different box sizes (28.47^3-98.47^3Å^3). The density, mole fraction of H_2 and temperature was kept constant at ρ = 5.22 kg/m^3, X_{H_2} = 0.98 and 3639K. Here, the system size was tested by finding the smallest box size where the enthalpy still showed intensive properties (properties that are independent of the system size). At that box size the partial molar enthalpy and the TCF were calculated at different temperatures (139-3639K). An extrapolation was performed twice. The first time was on the partial molar enthalpy and the TCF values to obtain the values at the thermodynamic limit. The second time was on the thermodynamic limit values so that the values could be scaled to higher temperatures.

The average over the entire time frame was used to calculate the thermodynamic properties for each system.

4.2.2. Reactive ReaxFF

The ReaxFF was simulated at different temperatures (3639-20796K) with density ρ=5.22 kg/m^3 (the same conditions as Skorpa *et al.[7]*). From these simulations all the thermodynamic parameters were obtained. For a system with a reactive force field, however, the topology is not known since the system continuously forms and breaks bonds. Consequently, additional codes were implemented post modelling using the trajectory file.

The first code created was used to calculate the MSD in 24 time steps. Here only atoms and molecules that did not react in that time frame were used. From the results the diffusion coefficient was obtained and compared with kinetic gas theory.

The second code was used to distinguish between atoms and molecules using the *Euclidean distance*. If the distance between two atoms was equal or less than 1.8 Å they were considered a molecule, resulting in two new trajectory files; one for the atoms and one for the molecules. With this code were the thermodynamic properties (except for the TCF and MSD) calculated as shown in the Chapter 2. When calculating the partial molar enthalpy and activation energy the output file, where the properties had been measured and stored at each 500 time step, was also used. Which time interval used depended on the property since the parameters are either calculated before or after equilibrium. The results were compared with results from the TBP simulations and the average bond enthalpy $\Delta H_{f,298K}$[35].

A third code was created to use the new trajectories from the second code. This was a new SSM code written in MATLAB to calculate the TCF. Here, 30 sub volumes (spheres) with a radius ranging from 0.05 L_t to 0.5 L_t were sampled 200 times.

To simplify the calculations, the hydrogen molecule was treated as an atom, creating a new atom *B* using the molecule's atom positons and the *center of mass*. Additional simplifications were performed on Equation(41) and (42) as shown below.

$$\Gamma_{H-B}^{-1} = \frac{\mathrm{cov}(N_B, N_H)}{\mathrm{mean}(N_H)} \tag{46}$$

$$\Gamma_{H-H}^{-1} = \frac{\mathrm{var}(N_H)}{\mathrm{mean}(N_H)} \tag{47}$$

Here, $\langle N_H^2 \rangle - \langle N_H \rangle^2$ represent the variance, *var*, $\langle N_H N_B \rangle - \langle N_H \rangle \langle N_B \rangle$ represent the covariance, *cov,* and *mean* is the arithmetic average. The values at the thermodynamic limit were found through extrapolation and compared with the results obtained using the FF and the TBP. The second and third code are found in Attachment D.

4.3. Interaction parameters

In Table 4.1 are the values for the parameters used when performing simulating with the FF. Here are the Morse potential values form the MM2 force field [36] and the Lennard-Jones from Delft Molecular Mechanics (DMM) force field [37]. The cut-off distance was set to 12.0 Å.

Table 4.1: Classical force field parameters [36, 37]

Morse potential	Lennard-jones potential
D_e = 4.747 eV	ε_{ij} = 27.655 K
a=1.946 $Å^{-1}$	σ = 2.63984 Å
r_0= 0.7414 Å	r_c = 12.0 Å

The parameters used when performing simulations with ReaxFF, were taken from the file *ffield.reax.cho* created by Chenoweth, van Duin and Goddard (2008) [5]. This file is provided by LAMMPS in the potential directory for the ReaxFF function.

The results from the TBP were obtained in Skorpa *et al*. (2014) [7] and the values she used are shown in Table 4.2. The cut-off distance was set to 2.8 Å.

Table 4.2: Three-body potential parameters used by Skorpa *et al.*[7]

Two particle-potential parameters	**Three particle-potential parameters**
$\alpha = 5.59 \times 10^{-21}$kJ	$\lambda = 2.80 \times 10^{-21}$kJ
$\beta_2 = 0.044067$ Å^p	$\mu = 0.132587$
$\gamma_2 = 3.902767$ Å	$\nu = -0.2997$
$p = 4$	$\gamma_3 = 1.5$ Å

5. Results and discussion

This chapter is divided into two sections depending on the interaction potential. First, the system is tested by the non-reactive FF. Then, the same system is used to calculate values with the reactive ReaxFF. The former is to conclude whether or not the system (the representation of hydrogen in a simulation box) is created accurately. The latter is to calculate thermodynamic parameters and compare it to the results in the Skorpa *et al.* paper[7]. Here, trends in the ReaxFF results are also commented on. To prevent repetition, both trends and comparisons will be commented on and discussed in this chapter. At the end of this chapter are the data processing and simulation parameters revised. The conclusion follows in Chapter 6.

It is worth mentioning that for the partial molar enthalpy and the TCF obtained with the SSM are inversely plotted. The purpose of this is to find the value at the thermodynamic limit, as explained in the Section 3.3.1. Moreover, temperature is a fixed parameter during the simulations. Since the temperature is dependent on the kinetic energy of the particles in the system it is, however, impossible to keep it constant over time. Thus, when the temperature is plotted in a graph, the mean value is used with the standard deviation (STD) represented as symmetrical error bars. Here, the STD is dependent on the interval used to calculate different parameters and therefore different STDs are used for the temperatures. Furthermore, since the temperature is fixed, the value stated in the input file is stated in this thesis, even though it is not correct to state such a specific number because of the uncertainties. Lastly, the data and equations used to calculate the theoretical self-diffusion coefficient using kinetic gas theory are found in Attachment A. The uncertainty propagation is calculated as shown in Attachment B. All the uncertainties are given with a single STD. An overview of the state variables and number of simulations is found in Attachment C. An example of a ReaxFF input is found in Attachment E.

5.1. Non-reactive classical force field

The system is tested an (N_j,V,T) ensemble with the non-reactive FF to see if the system is created properly in LAMMPS. Here, different thermodynamic parameters are calculated and compared with experimental values[34] and ideal gas. This is to see if the trends and values correspond. The ideal gas theory is in general accurate at low densities, ρ, pressures, p, and high temperatures, T [17]. In addition, the newly developed SSM code in LAMMPS is also going to be tested to see if heat capacity and the TCF yield close to ideal values.

5.1.1. Pressure

Figure 5.1, 5.2 and 5.3 show *p*, as a function of *T*, number of H_2, N_{H_2}, and mole fraction of H_2, X_{H_2}, respectively. The values are compared with ideal gas and/or experimental values[34]. In the first two figures the FF values are compared with experimental values and ideal gas. In both graphs, the experimental and ideal gas values are almost equal to the FF values. In Figure 5.1 the slope is equal for each plot. In Figure 5.2 the FF has a slope equal to 0.039, whereas the ideal gas and experimental values have 0.041 and 0.043, respectively. Thus, the deviation in the slopes is small. In Figure 5.3 is *p* calculated three different *T*; 100K, 300K and 500K. The slopes are -2.1,-3.3 and -4.6 respectively. The dotted lines are the ideal gas at each *T*. In this figure the values are close to ideal gas at low *T* and *ρ*.

To summarize the trends in Figure 5.1, 5.2 and 5.3, the values follow the same trend where the FF values are similar to ideal gas and experimental values at low *ρ* as expected. With an increase in *T* the fluctuations and the uncertainties increases, but the trend is constant. As the *ρ* increases, the gap between ideal and FF values increases. Arguably, the system created is a good representation of hydrogen atoms and molecules. The constant gap in Figure 5.1 can be explained by a higher *ρ* (3.35 kg/m^3). It is worth mentioning that *ρ* =3.35 kg/m^3 is a low *ρ* which explains why the deviations are small.

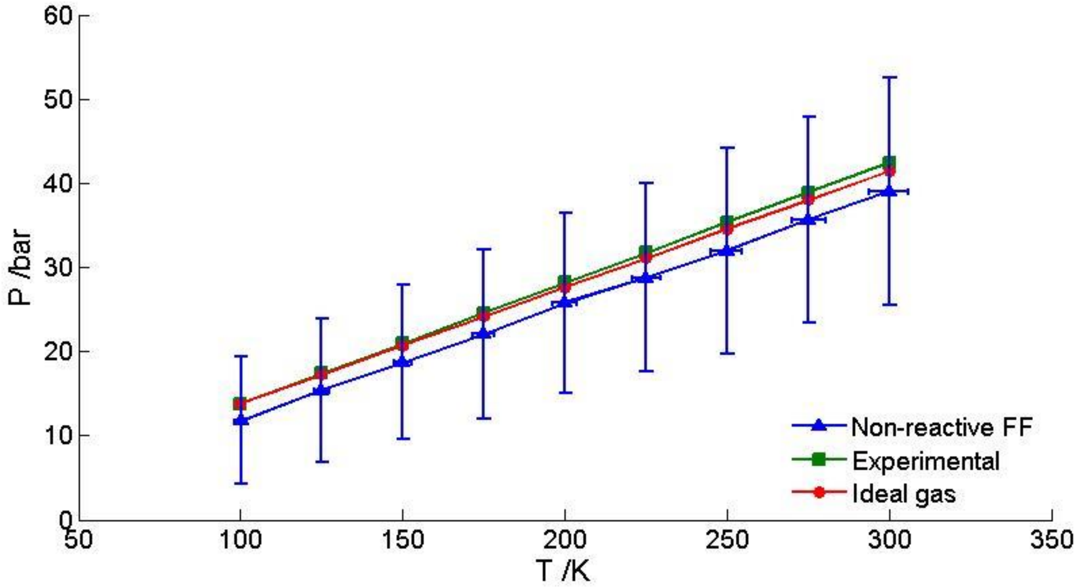

Figure 5.1: *p(T)* with the FF. Pressure (*p*) at different temperatures (*T*). The result is compared with experimental values [34] and ideal gas in a system at density, *ρ*=3.35 kg/m^3. Error bars are given in both x- and y-direction. Here are the slopes equal for each plot.

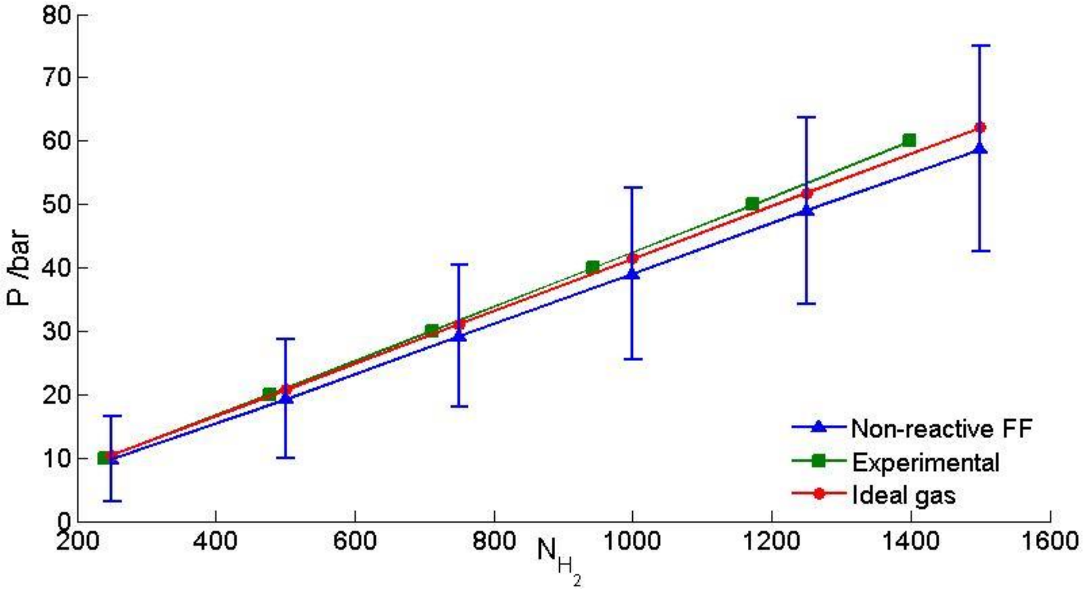

Figure 5.2: $p(N_{H_2})$with the FF. Pressure (p) at different number of H_2 (N_{H_2}).The results are compared with experimental values and ideal gas at 300K in a 100^3Å^3 sized box. Error bars are given in y-direction. As shown, the graphs have a positive slope.

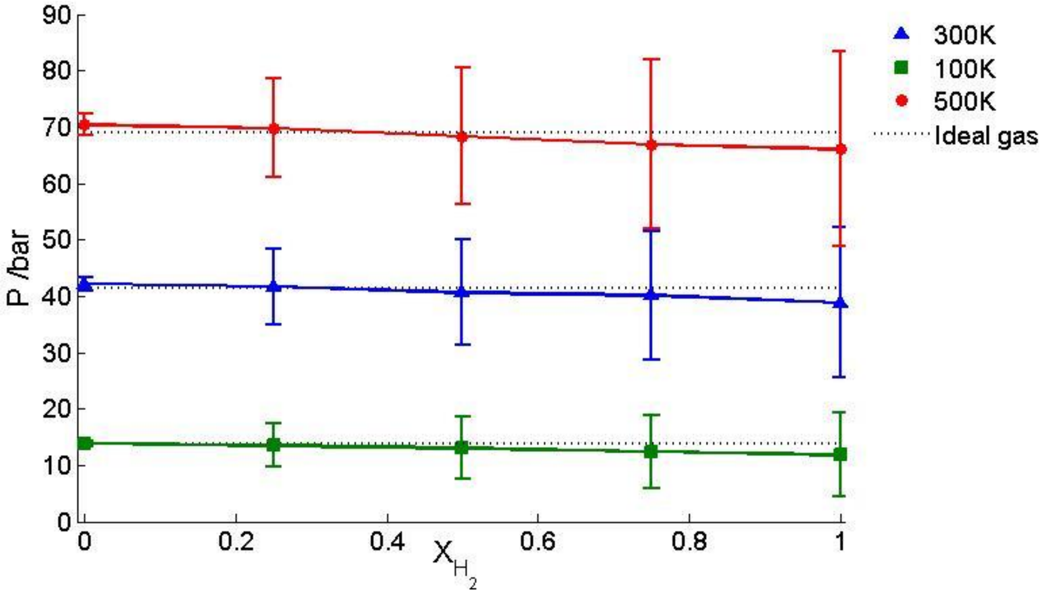

Figure 5.3: $p(X_{H_2})$with the FF. Pressure (p) at different mole fractions of H_2 (X_{H_2}). The result is compared with ideal gas at 100K, 300K and 500K in a 100^3Å^3 sized box with constant number of a 1000 particles. Error bars are given in y-direction. Here, the values for the ideal gas are constant and the FF values have a slight decrease as X_{H_2} increases.

On a side note: The increasing gap between the ideal values and experimental values, seen in both Figure 5.1 and 5.2 can be explained by the fact that performing experiments at high *p* and *T* is difficult. In Figure 5.1 all the experimental values are measurements of a supercritical fluid of hydrogen. The same fluid occurs at p>20 bars in Figure 5.2.

5.1.2. Diffusion

Figure 5.4 shows the MSD as a function of time, *t*, at different X_{H_2} and X_H. Here, the data has a linear trend where H has a greater MSD than H_2. Linear least squares regression was performed over the entire time interval for the pure components (X_i=1) to calculate the self-diffusion coefficient, $D_{self,i}$, using Equation(3). The results are shown in Table 5.1, where they are compared with the kinetic gas theory values, calculated with Equation (1.A) (see Attachment B). As mentioned in Attachment B, the tabulated values from H_2 and He are used to calculate the theoretical $D_{self,i}$ for H_2 and H, respectively. Compared with the theoretical values, D_{self,H_2} has a negative deviation of 3.3 % from the kinetic gas theory whereas $D_{self,H}$ has a negative deviation of 14.3%. Generally, $D_{self,i}$ for H is larger compared with H_2.

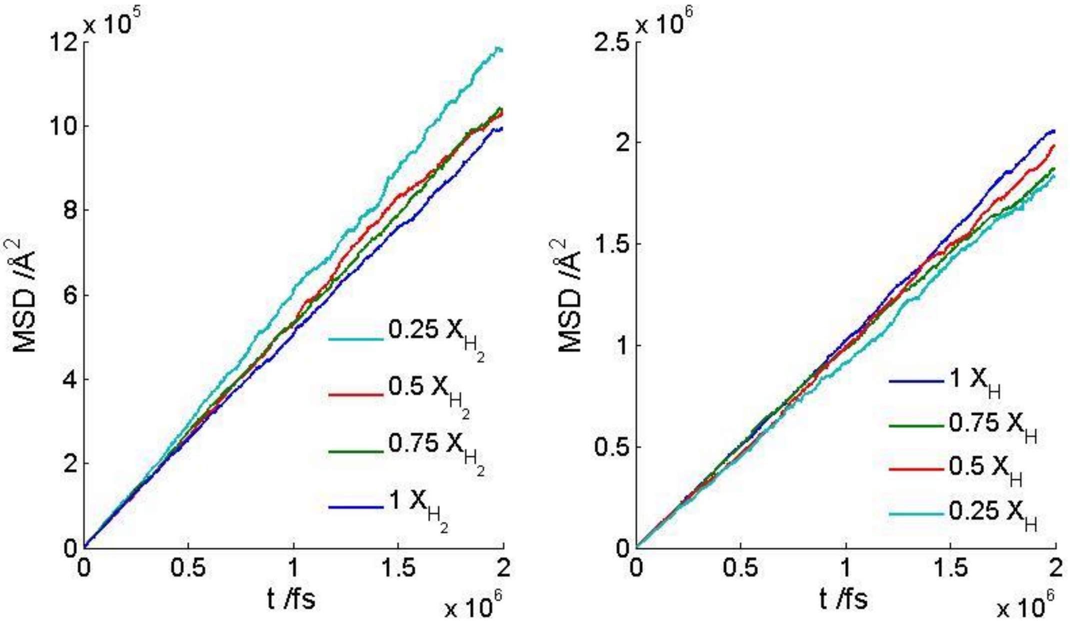

Figure 5.4: MSD(*t*) with the FF. Mean square displacement (MSD) as a function of time (*t*). Here the MSD is calculated at different mole fractions, for H_2 and H, (X_i) at 300K in a 100^3Å^3 sized box with constant number of a 1000 particles. As shown, the data have a linear trend and the values for H are larger than H_2.

Table 5.1: Self-diffusion coefficients ($D_{self,i}$) for H and H_2 with the FF calculated at 300K and compared with kinetic gas theory(the Chapman-Enskog theory) ($D_{self,i\ KGT}$) [12].Here, $D_{self,i}$ is calculated at different densities (ρ).

	$D_{self,i\ FF}$ [$10^{-6}m^2/s$]	$D_{self,i\ KGT}$ [$10^{-6}m^2/s$]	ρ [kg/m^3]
H	1.7407±0.0003	2.03±0.16	1.67
H_2	0.8312±0.0001	0.86±0.07	3.35

When calculating $D_{self,i}$, the result showed a larger value for H than for H_2. This is as expected since H is a “lighter” particle. There is a slight decrease in the MSD values as X_H decreases. This can be explained by the fact that the ρ increases. A greater ρ can affect the mean free path of the particles by making the system crowded and thus increasing the collision frequency, resulting in a smaller MSD. Furthermore, the values from the FF simulations have underestimated the $D_{self,i}$ compared with the kinetic gas theory. For D_{self,H_2} is the negative deviation in agreement with the trends found in Figure 5.1 where the values also had a small negative deviation for ideal gas and experimental values at ρ=3.35 kg/m^3. The larger underestimation of $D_{self,H}$ can, however be the result of using the tabulated values of He to calculate the theoretical self-diffusion coefficient. With this in mind one could conclude that the FF produces expected $D_{self,i}$ values.

5.1.3. Heat capacity

The newly developed SSM code in LAMMPS was tested by calculating the partial molar enthalpy, h_i, and the TCF, Γ_{ij}, in an (μ_j,V,T) ensemble. First, h_i was calculated for H and H_2 at different box sizes as shown in Figure 5.5. Here, h_i^{-1} is plotted against the inverse radius in reduced units, r^{*-1}, which is a fraction of the reservoir length, L_t, in the interval $0<r^*<0.5L_t$. The r^* is the same for all the systems whereas L_t is varied. As shown in both graphs, the h_i^{-1} has a steep positive slope at low r^{*-1} and then it stabilizes into a plateau as r^{*-1} increases. In the graph for h_H^{-1}do the calculations for each box size have the same trend. In the graph for $h_{H_2}^{-1}$, however, the values from calculations with box sizes lower than $48.5^3Å^3$ have a much higher peak then the rest right before the plateau is reached. Consequently, the box size $48.47^3Å^3$ was used to calculate h_i^{-1} at different T. The result is shown in Figure 5.6 where h_i^{-1} is plotted against the small system length, L. The relationship between r and the small system length, L, is shown in Equation(40).

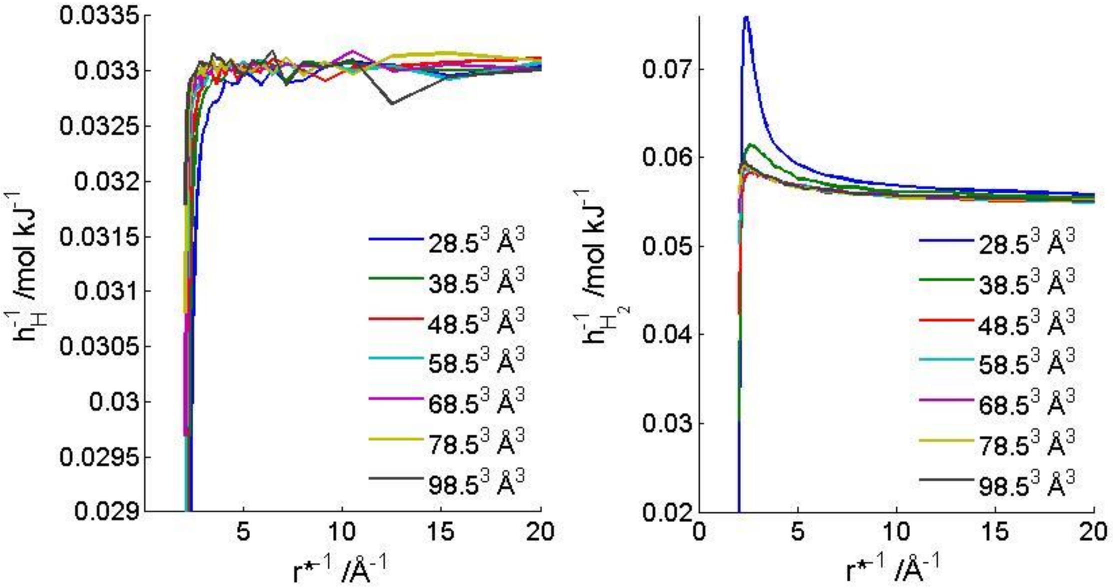

Figure 5.5: $h_i^{-1}(r^{*-1})$ at different box sizes with the FF. The inverse partial molar enthalpy (h_i^{-1}) was calculated using the SSM at different box sizes in a system with constant density, ρ=5.22kg/m^3, and mole fraction, X_{H_2}=0.98 at 3639K. The r^{*-1} is the radius to the sub systems in reduced units. As shown, the enthalpy is similar for each size, except for the box sizes at 38.47^{3}Å^3 and smaller for H_2.

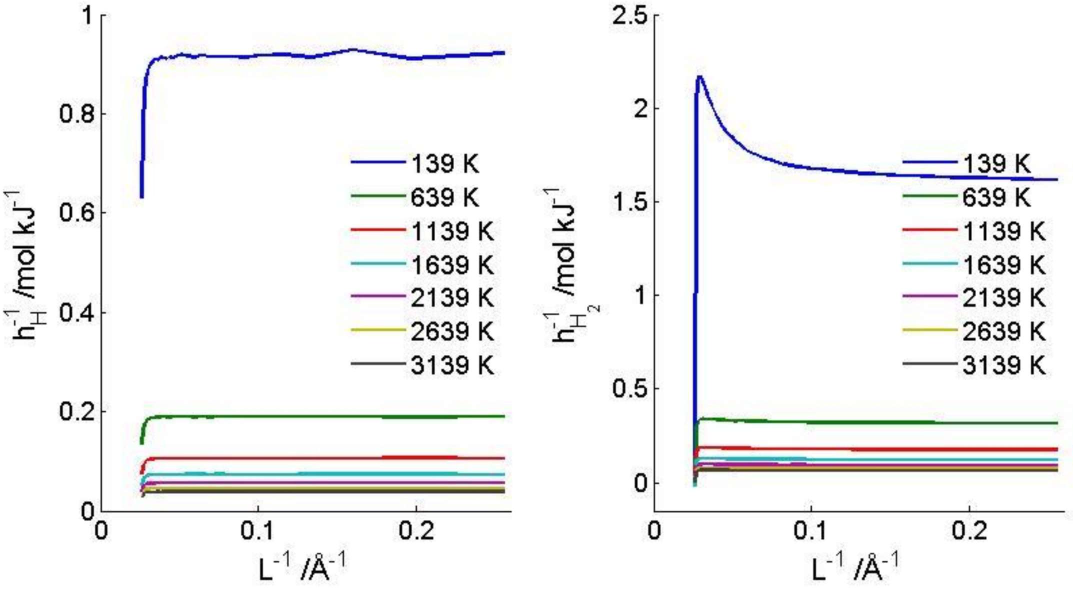

Figure 5.6: $h_i^{-1}(L)$ at different temperature with the FF. The inverse partial molar enthalpy (h_i^{-1}) was calculated as a function of the inverse small system length (L^{-1}), using the SSM at different temperatures in a system with constant density, ρ=5.22kg/m^3, and mole fraction, X_{H_2}=0.98. The graphs show that as the temperature increases, so does the partial molar enthalpy.

Each individual graph has the same trend as shown in Figure 5.5, but as T increases, h_H^{-1} decreases. This is expected since h_i is positively proportional to T. Extrapolation was performed on the interval $0.0825 \leq L^{-1} \leq 0.2550$ for every data set in both graphs in the figure. This was to obtain the value at the thermodynamic limit, $h_{i,\infty}$, as shown in Equation (45). The result is shown in Figure 5.7.

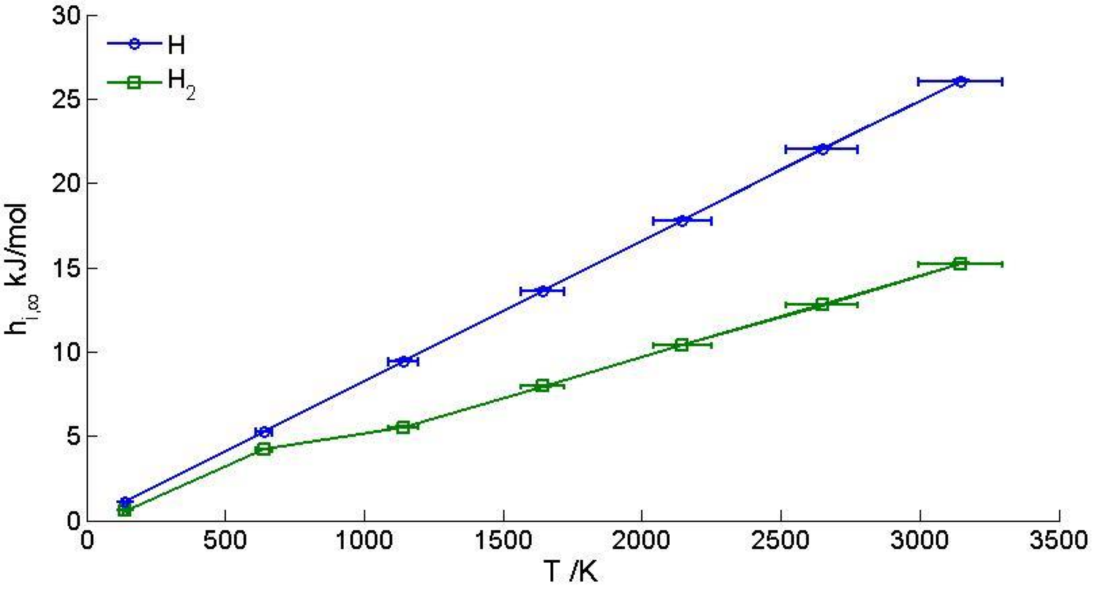

Figure 5.7: $h_{i,\infty}(T)$ with the FF. The partial molar enthalpy at the thermodynamic limit ($h_{i,\infty}$) calculated in a system with constant density, ρ=5.22kg/m^3, and mole fraction, X_{H_2}=0.98. The values were found through extrapolation of the partial molar enthalpy values for at different temperatures found using the SSM. Error bars are given in both x- and y-direction.

As shown in Figure 5.7, the values have a linear trend with a small error in T that grows as T increase. This is the same trend that occurs in previous graphs. In addition, the error for $h_{i,\infty}$ is so small it cannot be seen on the graph. The molar heat capacity ($C_{p,i}$) was found for the values in Figure 5.7 using linear least squares regression on the interval $139 \leq T \leq 3139$ and $1139 \leq T \leq 3139$ for H and H_2, respectively. The result is shown in Table 5.2.

Table 5.2: The molar heat capacity ($C_{p,i}$) of H and H_2 calculated with FF. The system is calculated at density, ρ=5.22kg/m^3 and is compared with the values from ideal gas[17].

	C_{p,H_2} [J/mol K]	**$C_{p,H}$[J/mol K]**
FF	4.83±0.008	8.337±0.018
Ideal	37.41	20.75

Here, $C_{p,H}$ is greater than C_{p,H_2}. This is not as expected. In addition to this unexpected trend the values are significantly lower than the ideal values. Based on these results the SSM code was revised and an error was found; the code could not recognize the molecules.

When testing the SSM code, the goal was to first find the smallest box size where h_i still showed intensive properties. This was done to gain insight into the SSM, and to shorten the simulation time by avoiding calculations on larger systems. The size of the system is irrelevant when it comes to comparing values with macroscopic properties, since the thermodynamic properties could be scaled from any nano-scaled system, using the thermodynamic limit. Since the only change between the different plots in Figure 5.5 is the system size, one can conclude from the plots of h_i for H_2 that below 48.5^3Å^3 the system size is no longer intensive. The error in the SSM makes, however, this result unreliable. For h_H in Figure 5.5 one could argue that the values show intensive properties in box sizes greater than 28.5^3Å^3.

As seen in Table 5.2 the $C_{p,i}$ values from the FF were simulations significantly smaller than the ideal values. The small value for H_2 was because of an error in the SSM, however this is not the case for H since the code did not affect its calculations. Here, $C_{p,H}$ deviated -60% from the ideal value. Previous result shows that the FF calculations are smaller than ideal values at greater ρ. Consequently, a smaller $C_{p,i}$ for FF compared with ideal values was expected. The deviations had, however, not been that large. Thus, an additional h_H calculation was performed in LAMMPS without using the SSM to check if the small $C_{p,H}$ was a result of an error in the code as well. Here, the internal energy was used, same as in the SSM. The LAMMPS simulations yielded the same $C_{p,H}$, which indicates that the FF is not an accurate interaction potential. When using the enthalpy to calculate $C_{p,H}$ it yielded ideal values.

5.1.4. Thermodynamic correction factor

Since the h_{H_2} values were incorrect, the TCF was only calculated for H, Γ_{HH}. The result is found in Figure 5.8. Here, the system is the same as used in Figure 5.6. Notice that the values have the same trend as h_H, only here, the values goes towards unity. Through extrapolation at the interval $0.15 \leq L^{-1} \leq 6.79$ Å^{-1} the value at the thermodynamic limit was obtained as shown in Equation(44). The result is found in Table 5.3.

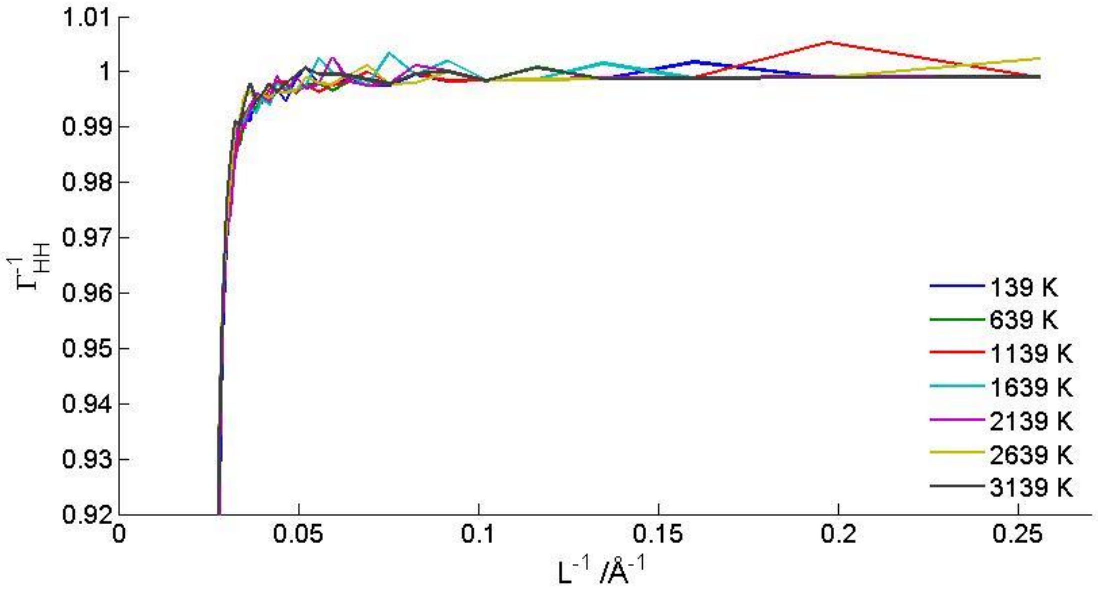

Figure 5.8: Γ_{HH}^{-1} (L^{-1}) at different temperatures with the FF. The inverse correction factor (Γ_{HH}^{-1}) calculated, as a function of the inverse small system length (L^{-1}), using the SSM in a system with density is, ρ=5.22kg/m^3. Here, the values go toward 1 as the L^{-1} increases for every temperature

Table 5.3: The thermodynamic correction factor at the thermodynamic limit. Calculated at different temperatures calculated for the FF system an (μ_j,V,T) ensemble at density, ρ=5.22kg/m^3.

T [K]	$\Gamma_{HH,\infty}^{-1}$
139±7	0.976±0.004
639±30	0.977±0.005
1139±55	0.984±0.007
1639±79	0.975±0.005
2139±100	0.976±0.005
2639±130	0.980±0.004

As shown, the TCF yielded values close to 1, which means that the system is close to ideal. This is in agreement with the results from the MSD and p calculations.

5.2. Reactive ReaxFF

The reactive ReaxFF was implemented in the system tested in Section 5.2; replacing the non-reactive FF. Six simulations were then performed with the same ρ and T as Skorpa *et al.*[7] The degree of dissociation of H_2 and the calculated p is seen in Table 5.4. Using these values, in addition to the trajectory and output files from the simulations, all the desired thermodynamic properties were obtained.

Table 5.4: Data collected from ReaxFF simulations at different temperatures. Here the number of particles (N_i) and total pressure (p) at density, ρ=5.22kg/m^3 is given.

T	**3639±30**	**7799±70**	**10398±100**	**12998±100**	**15597±140**	**20796±130**
$\mathbf{N_H}$	21±6	220±6	452±9	598±15	674±14	780±14
$\mathbf{N_{H_2}}$	490±3	390±3	274±5	201±8	163±7	108±7
p[bar]	800±104	1990±140	3290±120	4500±130	5700±120	8000±100

Additional testing was performed to verify that the new force field was correctly implemented. Here, the MSD and the activation energy, E_a, were calculated and compared with kinetic gas theory and the average bond energy, $\Delta H_{f,298K}$, respectively. After the testing produced desirable results, e.g. the MSD behaved as expected and E_a was close to the $\Delta H_{f,298K}$, the ReaxFF was used to calculate several thermodynamic parameters. As mentioned, the purpose of this thesis is to reproduce results from the Skorpa *et al.* paper[7] and conclude if the same results can be obtained with the ReaxFF. In other words, test if the ReaxFF and the TBP produces close to equal results.

5.2.1. Diffusion

Figure 5.9 shows MSD calculated for H_2 and H at different temperatures. By zooming in on the origin in Figure 5.4, the same slope would be found. This slope is caused by the coupling constant Q as mentioned in Section 3.1.2. The reason why it is not visible in the former figure is that the graph consists of 2,000,000 time steps, whereas the graph in the latter consists of 12,000. Thus, the two figures are consistent. Additional information gained from Figure 5.9 is that, as expected, the MSD increases with T. An unexpected trend is, however, that the MSD for H_2 at 7799K and 10398K looks like they are overlapping. Despite what is shown in the graph the values are close but not equal, where the MSD values at 7799K are smaller. Thus, the trend that the MSD increases with T is consistent in both graphs. The MSD for H at 3639K is neglected since there were not enough atoms present in the system.

Linear regression was performed on the interval $600 \leq t \leq 1200$ to achieve $D_{self,i}$. The result is shown in Figure 5.10 where it is compared with the kinetic gas theory (KGT) calculated with Equation (1.A) (see Attachment B).. Here, $D_{self,H}$ is larger than D_{self,H_2} as expected. Moreover, the kinetic gas theory is smaller. No tabulated values for H were available at such high temperatures; hence, the theoretical values for H_2 could not be calculated. The error bars in x-direction are so small they do not show on the graph.

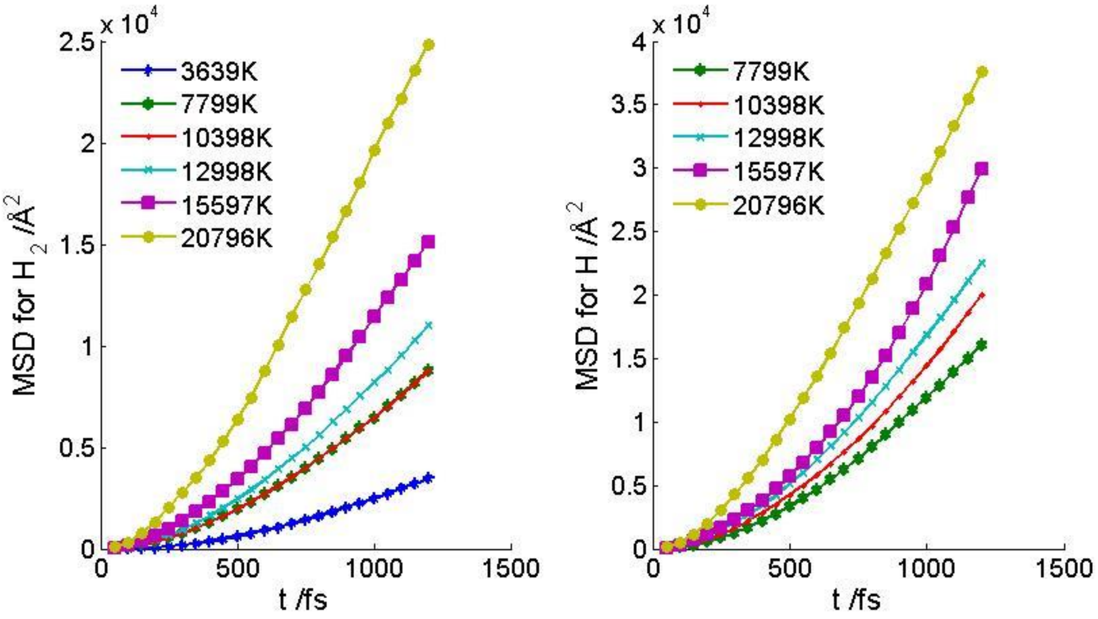

Figure 5.9: MSD(*t*) with the ReaxFF. The mean square displacement (MSD) for H and H_2 as a function of time (*t*) were calculated different temperatures at density, ρ=5.22kg/m^3. As shown is data linear, expect for the small slope around zero. The MSD for H_2 at 7799K and 10398K overlap.

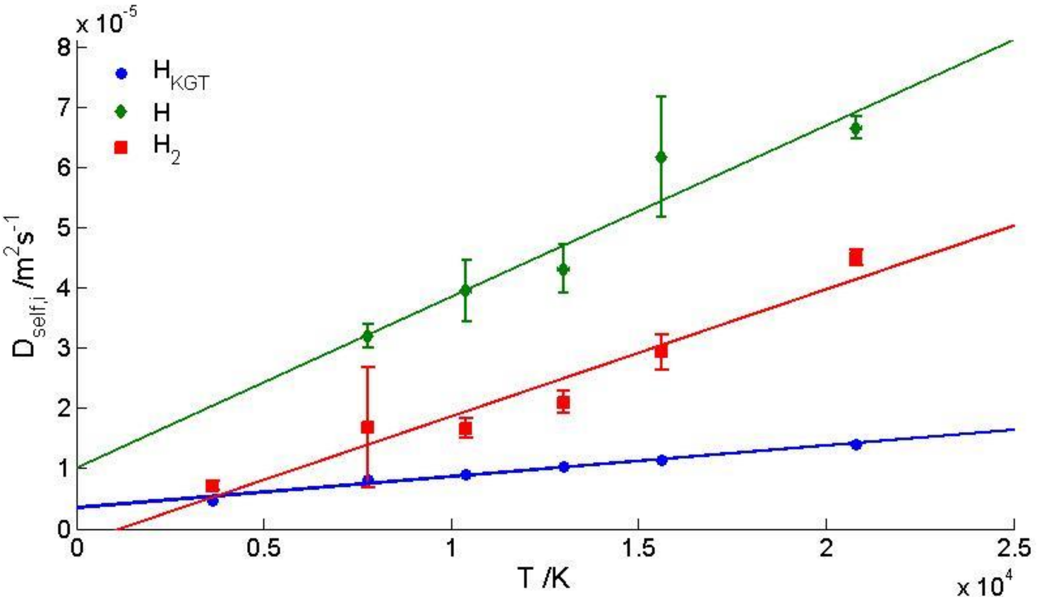

Figure 5.10 $D_{self,i}(T)$ with the ReaxFF. The self-diffusion coefficient ($D_{self,i}$) is calculated for H and H_2 and compared with kinetic gas theory (KGT) at different temperatures (*T*) at density, ρ=5.22kg/m^3. Error bars are given in y- and x- direction.

In Figure 5.10 the theoretical $D_{self,H}$ from the kinetic gas theory is smaller than $D_{self,H}$ calculated with ReaxFF. This can be a result of using the tabulated values for He as mentioned earlier or that the theory is not valid at such high T. In addition, the kinetic gas theory has tabulated data from diluted gases. The system with ReaxFF has a ρ=5.22 kg/m^3 and, thus, is not as a diluted system. The $D_{self,i}$ values calculated for a system with FF at 300 K were closer to the kinetic gas theory values had a ρ = 3.35 kg/m^3. Thus, it is possible to conclude that the MSD is as expected since the MSD increased as a function of T and t. And $D_{self,i}$ was larger for H compared with H_2.

5.2.2. Heat capacity

At constant (N_j,V,T) was h_i calculated using LAMMPS at T = 3639K-20796K. Here, the values were averaged over the interval 101,600fs≤t≤102,650fs. At this interval the systems for each T were at equilibrium. An example of h_i at 15597K is given in Figure 5.11. Here there are still some fluctuations, even though the system is stable. The plot at other T shows the same trend. Figure 5.12 shows averaged h_i as a function of T compared with $h_{i,\infty}$ calculated at constant (μ_j,V,T) from the TBP and the non-reactive FF simulations. The latter was found through extrapolation of the graph in Figure 5.7. The general trend in Figure 5.12 is that that at low T h_H is higher compared with h_{H_2}. But as T increases h_{H_2} exceed h_H because it has a larger slope. Furthermore, the values for h_H from the ReaxFF and the TBP simulations are close to parallel at high T (T≥10398), whereas for the values for h_{H_2} are close to similar at low T (T≤12998K). Based on these intervals $C_{p,i}$ was calculated using linear least squares regression. The results were compared with the TBP and the FF simulation values in addition to ideal values. The results are shown in Table 5.5. Here, the ReaxFF and the TBP express the same trends. For both force fields C_{p,H_2} is larger than for $C_{p,H}$. By comparison the $C_{p,i}$ are values close and both are larger than ideal values, as expected. The values calculated with the ReaxFF have, however, higher uncertainty.

As mentioned above, the SSM was not used to calculate h_i. This resulted in values in another ensemble than the TBP, as seen in Figure 5.12. Here, the h_i calculated at constant (N_j,V,T) was compared with values at the thermodynamic limit at constant (μ_j,V,T). It was possible, however, to compare the values from different ensembles since ρ was low . As mentioned in Section 2.5 previous studies by Skorpa *et al.* [7] has confirmed that the values at different ensembles at ρ=5.22 kg/m^{3}do not deviate significantly.

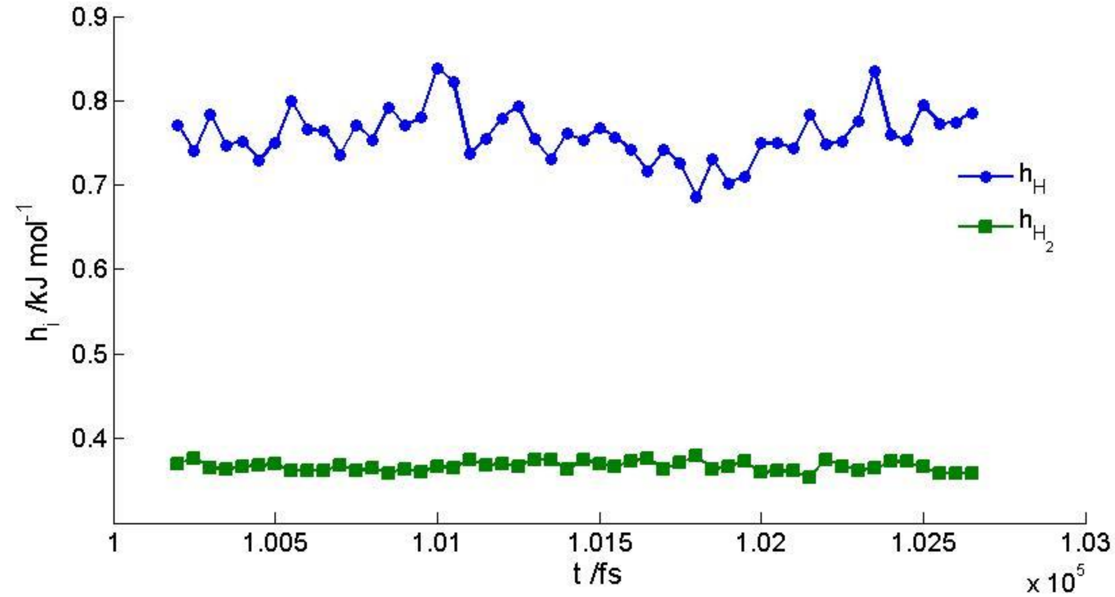

Figure 5.11: $h_i(t)$ with ReaxFF. Partial molar enthalpy (h_i) as a function of time (t) was calculated at 15597K at density, ρ=5.22kg/m^3. LAMMPS was used to calculate h_i for H and H_2, h_H and h_{H_2}, at the interval 600fs to 102,650fs. Error bars are given in both x- and y-direction. Even though the system is stable, fluctuations in the values do occur.

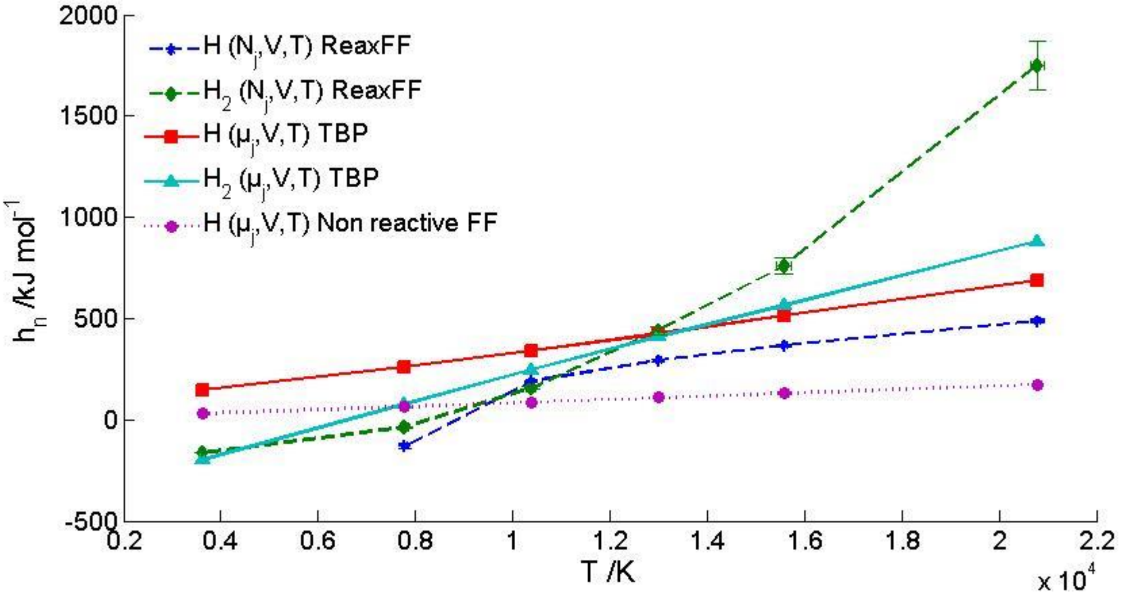

Figure 5.12: $h_i(T)$ with ReaxFF. The partial molar enthalpy (h_i) for H and H_2 calculated at different temperatures at constant (N_j,V,T) and is compared with $h_{i,\infty}$ calculated at the thermodynamic limit with SSM in at constant (μ_j,V,T) with the TBP and the FF. The values are at density, ρ=5.22kg/m^3.

Table 5.5: The heat capacity of H and H_2 with the ReaxFF. Compared with the values from ideal gas[17], FF and the TBP.

	C_{p,H_2} [J/mol K]	$C_{p,H}$[J/mol K]
Non-reactive FF	-	8.337±0.018
ReaxFF	63±13	28±3
TBP	62.8±0.7	31.7±0.7
Ideal	37.41	20.785

Furthermore, what is interesting about the plots in Figure 5.12 is that the h_H is close to parallel to the values from the TBP simulations only at high T, whereas the h_{H_2} are close to similar only at low T. This is further confirmed by the calculation of $C_{p,i}$ at these T intervals, which resulted in equal $C_{p,i}$ compared with the TBP values. Since they are in different ensembles some deviation is expected, however this particular trend can arguably be explained by the degree of dissociation. At high T the dissociation is high, thus the N_H is high. At low T, similarly, the dissociation is low, thus the N_{H_2} is high. These trends indicate that the ReaxFF is dependent on the number of particles to create accurate calculations. In other words, when there are many particles of a species, the partial calculations are more accurate. This conclusion is drawn based on the assumption that the TBP calculations are accurate. Here, the FF values were not used in the comparison because they were low and, as previously concluded, the interaction potential might not be accurate since it deviates significantly from the ideal values.

It is worth mentioning that the $C_{p,i}$ calculations have significantly higher uncertainty compared with the TBP values. This can be an effect of the post modelling calculations where the N_{H_2} was determined with an additional code (code no. 2) and that h_i was only averaged over 50 time steps after equilibrium. It can, however, be an indication that the ReaxFF is a less accurate interaction potential than the TBP, as expected. More likely, it is a combination of the two.

5.2.3. The thermodynamic correction factor

The TCF was calculated using the SSM at constant (μ_j,V,T) at T= 3639K-20796K. An example of such a calculation is shown as a graph in Figure 5.13, where Γ_{HH}^{-1}, $\Gamma_{HH_2}^{-1}$ and $\Gamma_{H_2H_2}^{-1}$ are plotted against L^{-1} at 15597K. Here, the Γ_{ii} for both particles have the same trends as the h_i calculated with the SSM, except the plateau is reached when the values for Γ_{ii}^{-1} is close to unity. The values go toward zero for $\Gamma_{HH_2}^{-1}$. This is as expected. The plot at the other

T shows the same trend. Through extrapolation at the interval 0.0633 $Å^{-1} \leq L^{-1} \leq 0.1812 Å^{-1}$ was the thermodynamic limit obtained for each *T*. In addition, extrapolation was performed on Γ_{HH}^{-1} form the FF simulations, to make it valid at higher temperatures. The results are found in Table 5.6 and are plotted in Figure 5.14.

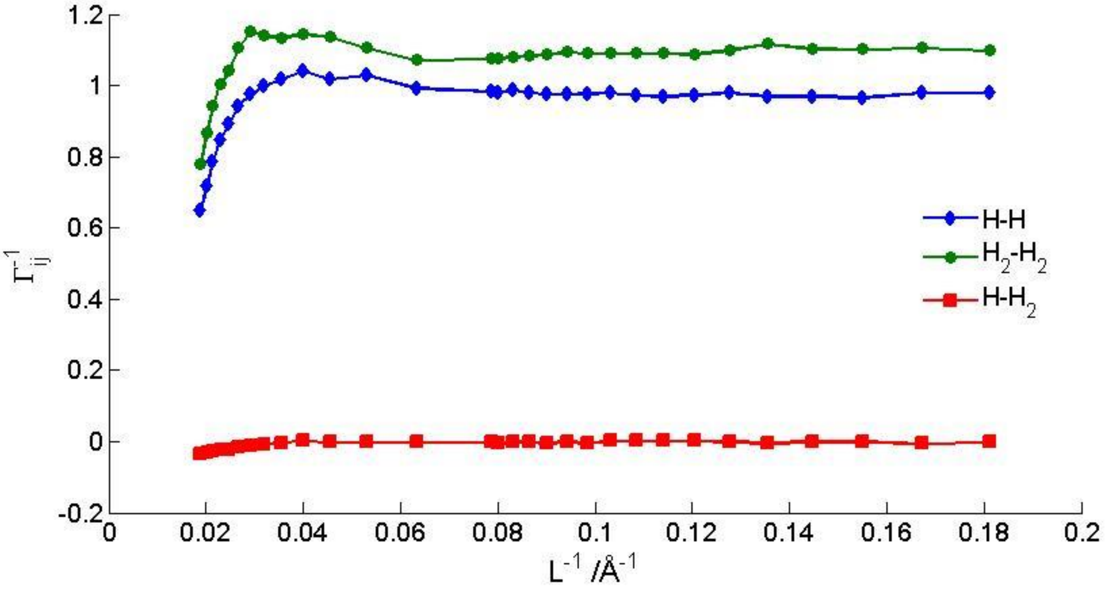

Figure 5.13: $\Gamma_{ij}^{-1}(L^{-1})$ with the ReaxFF. The inverse correction factor (Γ_{ij}^{-1}) as a function of the inverse system length (L^{-1}) at 15597K and at density, ρ=5.22kg/m^3 is calculated. Here, the Γ_{ii}^{-1} goes toward one as the small system length increases, whereas Γ_{ij}^{-1}goes toward zero.

Table 5.6: The thermodynamic correction factor at the thermodynamic limit ($\Gamma_{ij,\infty}^{-1}$) . Calculated using different force fields at constant (μ_j,*V*,*T*), at density, ρ=5.22kg/m^3.

	ReaxFF			TBP			FF
T	$\Gamma_{HH,\infty}^{-1}$	$\Gamma_{HH_2,\infty}^{-1}$	$\Gamma_{H_2H_2,\infty}^{-1}$	$\Gamma_{HH,\infty}^{-1}$	$\Gamma_{HH_2,\infty}^{-1}$	$\Gamma_{H_2H_2,\infty}^{-1}$	$\Gamma_{HH,\infty}^{-1}$
3639	2.12±0.03	-0.07±0.03	0.945±0.004	1.00	-0.00	0.87	0.976±0.004
7799	1.14±0.01	0.018±0.005	0.907±0.007	1.00	-0.04	0.91	0.977±0.005
10398	1.002±0.004	0.025±0.004	1.022±0.006	0.98	-0.08	0.94	0.984±0.007
12998	0.966±0.003	0.007±0.002	1.023±0.003	0.96	-0.09	0.97	0.975±0.005
15597	0.965±0.008	-0.007±0.002	1.115±0.007	0.96	-0.12	0.97	0.976±0.005
20796	0.960±0.005	0.008±0.002	1.14±0.01	0.94	-0.11	0.99	0.980±0.004

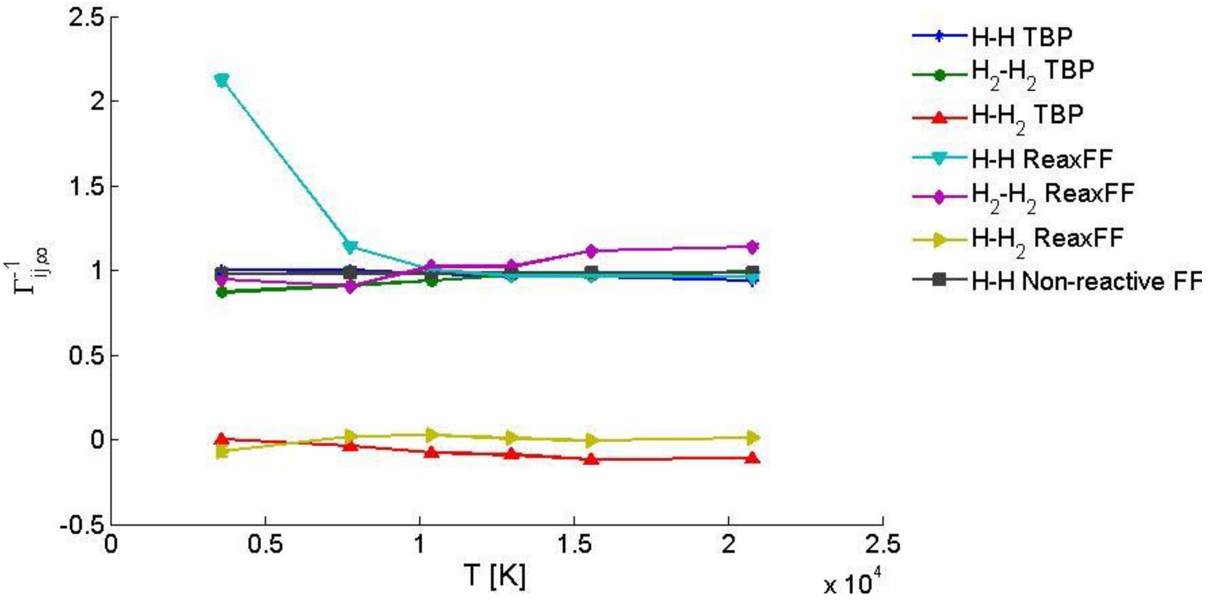

Figure 5.14: The correction factor at the thermodynamic limit with RreaxFF. The inverse of the thermodynamic correction factor for H and H2, ($\Gamma_{ij,\infty}^{-1}$)calculated with FF, ReaxFF and TBP at different temperatures(T) at density, ρ=5.22kg/m^3. Error bars are given in both x- and y-direction. Here, the $\Gamma_{ii,\infty}^{-1}$is around 1, whereas $\Gamma_{ij,\infty}^{-1}$is around 0.

As shown, the values for FF are close to ideal and linear. This is consistent with the results in Section 5.1. The TBP and the ReaxFF values have, compared with each other, the similar trends, except for the ReaxFF values at T≤7799 and at T≥15597 where $\Gamma_{HH,\infty}^{-1}$ and $\Gamma_{H_2H_2,\infty}^{-1}$, respectively, deviate positively. This is within the intervals that h_i deviated from the TBP values, as seen in Figure 5.12. This is in agreement with the hypothesis that the ReaxFF is dependent on the number of particles to create accurate calculations. An additional factor that can have affected the TCF values is the difference in sampling when using the SSM. In the TBP simulations, Skorpa *et al.*[7] sampled 50 spheres per radius at every 100 time step and time averages were calculated at every 10,000 time step. In this thesis, using LAMMPS in combination with the SSM code developed in MATLAB, were 200 spheres per radius sampled at every 500 time step and time averages were calculated over 50 time steps. The code was tested at longer runs, but the TCF graphs seem unaffected. The sampling amount, on the other hand, improved the smoothness of the graph significantly. In other words, it is possible to improve the SSM results by increase the number of radiuses used and number of sampling. As mentioned, it is, however, expected that the ReaxFF is less accurate than the TBP.

From the trends in Table 5.6, the $\Gamma_{HH,\infty}^{-1}$ decrease with T as N_H increase and $\Gamma_{H_2H_2,\infty}^{-1}$ increase with T as N_{H_2} decrease. Both values are around one. The interaction between a component and itself is one in an ideal system. The results are consistent with Skorpa *et al*. The $\Gamma_{HH_2}{}^{-1}$ values for the ReaxFF and the TBP differ in signs, however, both have small values that are around zero. That the $\Gamma_{HH_2}{}^{-1}$ goes toward zero indicates the coupling between H and H_2 is very small.

5.2.4. Heat of reaction, equilibrium constant

Assuming that the dissociation of H_2 is a first order reaction, E_a was calculated in accordance with Equation(7). Here, the reaction constant, k_r at a given T was found through linear least square regression performed on the plot of the natural logarithm of the change in concentration (N_{H_2} divided by the initial amount, $N_{H_2}{}^0$) as a function of t, as shown in Equation(8). The k_r was calculated for five out of the six ReaxFF simulations. The simulation at 3639K was neglected since the dissociation was low (2.1%). Figure 5.15 shows an example of such a plot at 12998K. The plot is similar at for the other T.

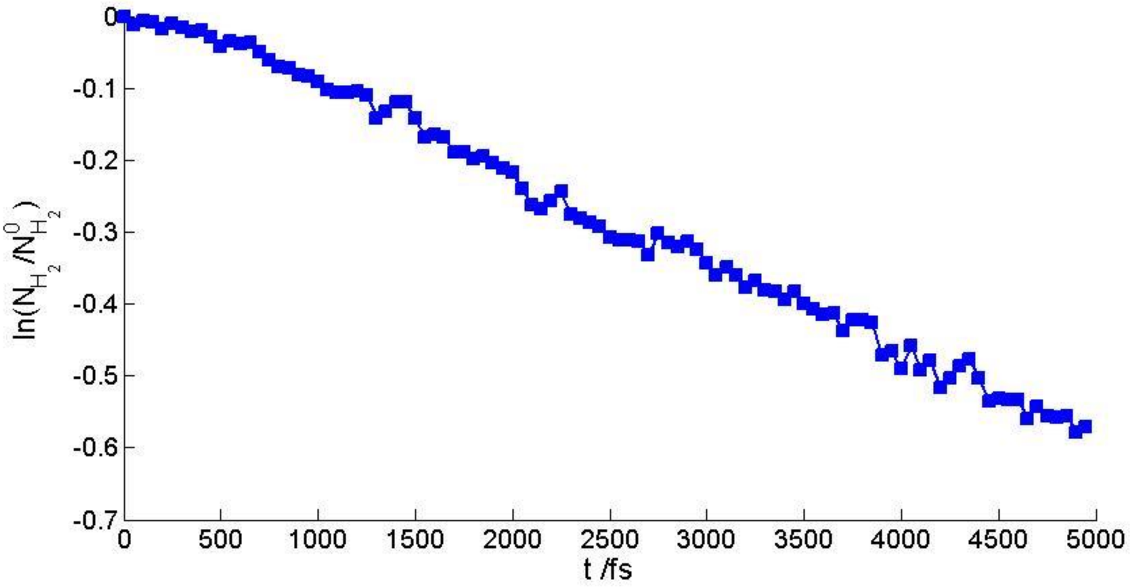

Figure 5.15: Finding the reaction constant for ReaxFF. The natural logarithm of the number of H_2 (N_{H_2}) divided by the initial amount ($N_{H_2}{}^0$) as a function of time (t) at 12998K at density, ρ=5.22kg/m^3. The graph shows that the dissociation of H_2 is a 1st order reaction.

A detailed overview of the intervals used in the regression and results of the calculated k_r at each T is shown in Table 5.7. Different time intervals were used since k_r has to be calculated before the system reaches equilibrium. As seen, the system reaches equilibrium faster at higher T, as expected.

Table 5.7: The reaction constant (k_r) for the ReaxFF. Calculated through linear least square regression at different temperatures (T), at density, ρ=5.22kg/m^{3}and at varying time intervals

T [K]	Time interval [10^3fs]	k_r [10^{-5}/fs]
7799±500	0-20	0.77±0.013
10368±1000	0-10	3.88±0.03
12998±1700	0-5	12.17±0.010
15597±3000	0-2.45	22.0±0.4
20796±4000	0-2	51.4±0.6

The result from Table 5.7 was plotted in Figure 5.12. Here, $\ln k_r$ is plotted as a function of $1/T$, which was used to obtain E_a. The result is found in Table 5.8, where the value is compared with the $\Delta H_{f,298K}$[35].

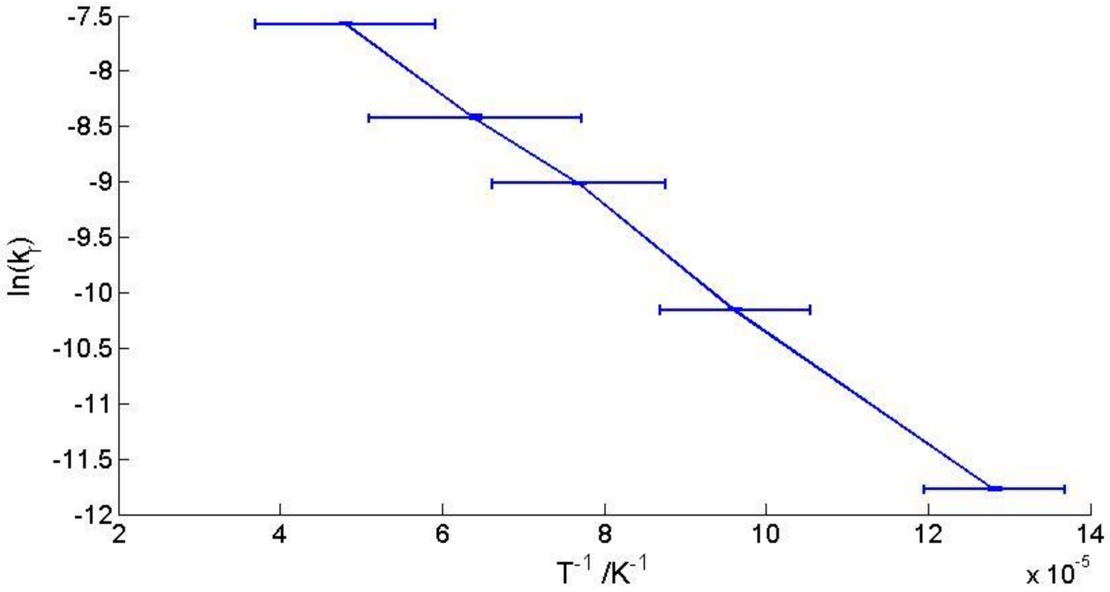

Figure 5.16: Finding the activation energy for ReaxFF. The natural logarithm of the reaction constant ($\ln k_r$) as a function of inverse temperature (T^{-1}) . Error bars are given in both x- and y-direction. Linear least squares regression was preformed to obtain the activation energy.

Table 5.8: The activation energy (E_a) for ReaxFF. The result is compared with the average bond enthalpy for H_2 ($\Delta H_{f,298K}$)[35].

Parameter	**[kJ/mol]**
E_a	438±9
$\Delta H_{f,298K}$	436

To conclude, the downward linear trend in Figure 5.15 confirms our assumption that the dissociation of H_2 was first order reaction. Here, the E_a deviates less than 0.5% compared with the average bond enthalpy $\Delta H_{f,298K}$[35] where the latter is in the uncertainty interval of the former. In other words, they are, arguably, equal.

The X_{H_2} was calculated using the values in Table 5.4 for T=3639-20796K. The result is shown in Figure 5.17 where the values are compared with the values from the TBP simulations. Here, the X_{H_2} for both force fields are close to equal. Moreover, the error bars are so small that they are barely visible in the plot. From the X_{H_2} and X_H were the dissociation constant, K_x, calculated as shown in Equation (14).

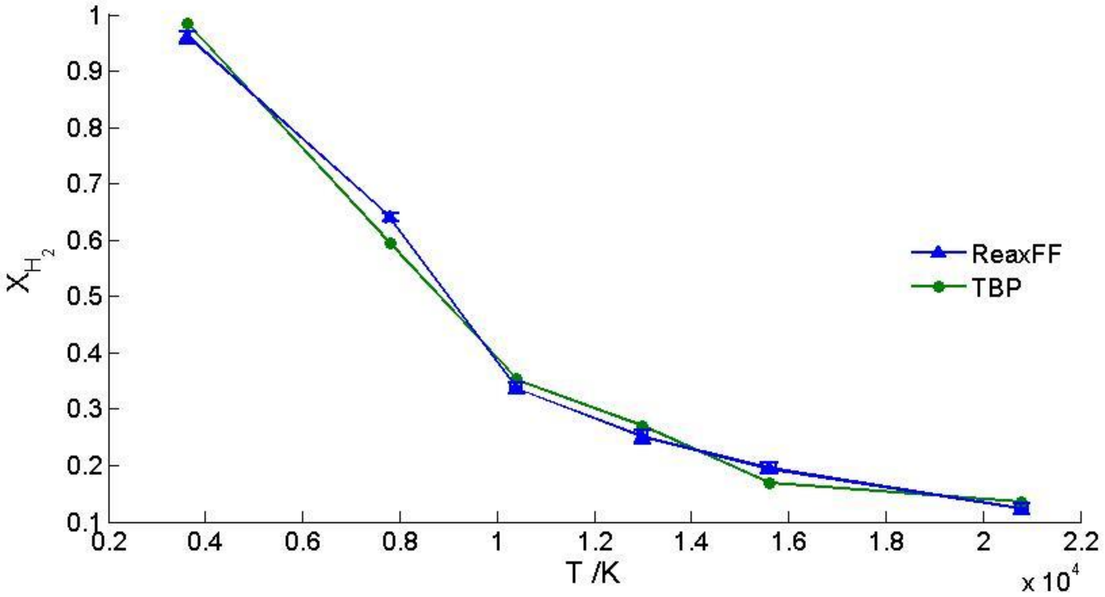

Figure 5.17 Dissociation of H_2. The mole fraction of H_2,(X_{H_2}) at different temperatures(T) calculated with ReaxFF and compared with results from TBP simulation at density, ρ=5.22kg/m^3. Error bars are given in both x- and y-direction. As shown, the values for the two force fields close to equal.

To gain the reaction enthalpy, $\Delta_r H_{ReaxFF}$, $ln(K_x)$ was plotted against $1/T$ as shown in Figure 5.18. A linear least squares regression was performed to obtain $\Delta_r H_{ReaxFF}$ as shown in

Equation(13). The result is shown in Table 5.9 where it is compared with $\Delta_r H_{TBP}$. Here, $\Delta_r H_{ReaxFF}$ deviates -4% from $\Delta_r H_{TBP}$

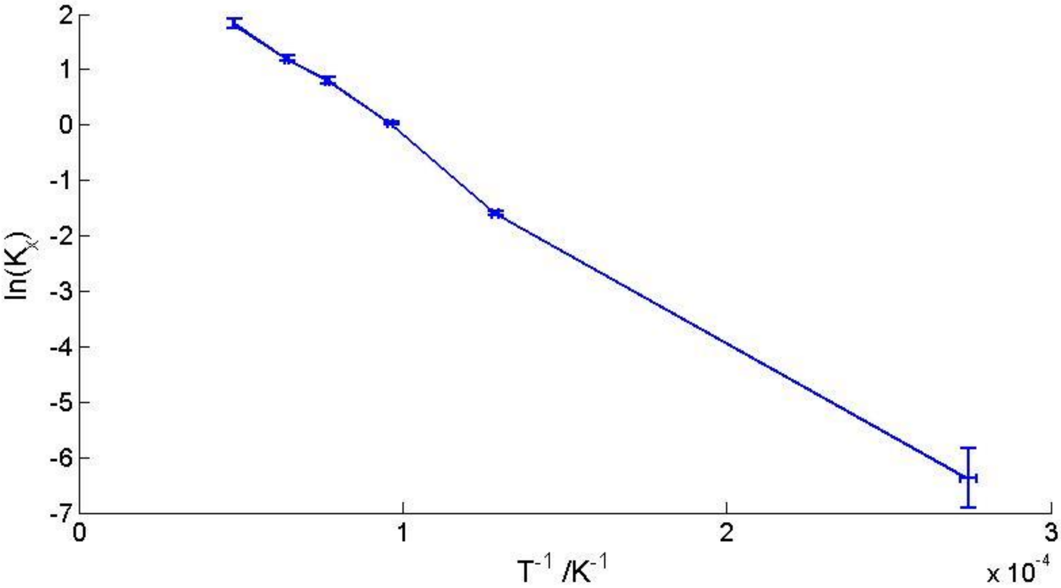

Figure 5.18: Finding the reaction enthalpy for ReaxFF. The natural logarithm of the dissociation constant (*ln* K_x) plotted as a function of the inverse temperature (T^{-1}). Error bars are given in both x- and y-direction. Since the plot was linear it was possible to preform linear regression to obtain reaction enthalpy.

Table 5.9: The reaction enthalpy (Δ_rH) for ReaxFF. Compared with the reaction enthalpy calculated with the TBP at density, ρ=5.22kg/m^3.

Parameter	**[kJ/mol]**
$\Delta_r H_{ReaxFF}$	302.0±1.2
$\Delta_r H_{TBP}$	316±3

As seen in Figure 5.17, the dissociation is close to equal for the two force fields. Here, the second code, mentioned in Section 4.2.2, used the distance 1.8 Å to determine if the atoms made a molecule. This distance was determined by studying at the radial distribution for the system at each *T*. As mentioned in Section 3.2.2 is the sigma bond between two atoms generally below ~1.5 Å and is negligible above ~2.5Å. The aim was not to alter the result gained with the ReaxFF in the post modelling phase by choosing an accurate distance. The fact that the reaction enthalpies were so close for both force fields indicates that the chosen distance was a reasonable choice.

5.3. A review of the data processing and simulation parameters

In this section are some general comments about the data processing and simulation parameters.

First, in Figure 5.12 and 5.14 the values from the FF simulations were extrapolated to T = 3639K-20796K. This was done because the non-reactive FF cannot be used at such high *T* since the simulation crashed. This is a result of the increase in distance between the atoms in a molecule as *T* increases due to dissociate.

Second, both h_i and the TCF were calculated using an additional code in MATLAB (code no. 2). This code was very time consuming and therefore only 50 time steps, after equilibrium, were used to calculate the parameters. Longer runs were tested on the TCF. Here, the values seemed unaffected by the simulation length. It was assumed that the time range was sufficient. In further work, h_i values might also have to be tested.

Third, in regards to simulations time, the TBP used about 24 hours on 7-10 million time steps (1 time step = 0.22 fs), whereas the ReaxFF used about 40 minutes on 1 million time steps (1 time step = 0.1 fs). Skorpa *et al*.[7] did, however, not use LAMMPS to perform the MD simulations so comparing the time used per simulation might not be accurate. By assuming that the different in time consumption between LAMMPS and their own developed program is small, it is possible to could conclude that the ReaxFF is faster.

Fourth, the simulation time, the number of simulations and time step are factors that can affect the accuracy of the calculations (as explained in Section 3.1.1). This thesis, however, tried to avoid these effects by matching the number of simulations to Skorpa *et al.[7]*, using the time step 1fs which has been proven optimal for ReaxFF simulations and making sure that the simulations had run long enough by checking if the equilibrium had been reached.

Lastly, some critique to the data processing methods used in this thesis. By performing many of the calculations post modelling some unnecessary uncertainties occurs. These include the counting of the molecules, not being able to calculate the partial molar enthalpy using the SSM, thus comparing values in different ensembles, and not calculating the thermodynamic parameters over longer time intervals due to time consuming calculations in MATLAB. A lot of these problems would have been avoided by implementing the SSM code directly in LAMMPS.

6. Conclusion and outlook

The aim of this thesis was to study the ReaxFF, combine it with the SSM and conclude whether or not it was feasible to use the ReaxFF instead of the TBP and still get reasonable results. This was done by performing in total 55 simulations in LAMMPS; 49 using the FF and 6 using the ReaxFF. The latter was processed with three additional codes, post-modeling.

To check if the system and the SSM code were implemented correctly they were first tested with the non-reactive FF. Based on the results from calculating p with different variables and the diffusion, it was concluded that the system was correctly assembled. Here, the results were equal to ideal gas and experimental values at low ρ, the MSD behaved as expected and $D_{self,i}$ yielded values close to kinetic gas theory. The SSM code was tested by calculating h_i and the TCF. Here, the code yielded $\Gamma_{HH,\infty}^{-1}$ values close to ideal, low $C_{p,i}$ values and an unexpected trend ($C_{p,H}>C_{p,H_2}$). Consequently, it was revised and an error was found that affected the values for H_2; the SSM code could not recognize the molecules. Thus, this code was not used in further calculations.

In short, the ReaxFF produced fast calculations, which were consistent with expected trends. Here, the $D_{self,H}$ was larger than D_{self,H_2}, whereas C_{p,H_2} was larger than $C_{p,H}$. Furthermore, the E_a was equal to $\Delta H_{f,298K}$ for hydrogen. Consequently, it was concluded that the ReaxFF was assembled correctly. By comparing the dissociation, h_i and the TCF with the values in Skorpa *et al.[7]* it was concluded that the ReaxFF compares to the TBP. Here, the ReaxFF and TBP values were equal, or close to equal. In general, the ReaxFF values had high uncertainty and deviated more from the TBP when the particle number was low. This was expected since the ReaxFF is a less accurate potential, however, it was argued that it could also be an effect of the post-modelling processing.

To conclude, the ReaxFF simulates hydrogen dissociation as expected. Furthermore, it is feasible to use the ReaxFF instead of the TBP. Despite the TBP being a more accurate potential, the ReaxFF produces close to the same values, is more applicable and faster.

The next step is to perform ReaxFF simulations with other chemical reactions to see if the same trends occur. In addition, it would be interesting to expand the ReaxFF simulations by performing a surface reaction with dissociation of H_2 on a palladium surface. Since the SSM code included an error, further work implies improving this code to minimize the uncertainties that comes with extensive post-modelling processing. In additions, the values in this thesis might be improved by calculating h_i, with the ReaxFF, at longer runs.

References

1. Allan, N.L., S. Stølen, and T. Grande, *Thermodynamics and materials modelling.* Chemical Thermodynamics of Materials: Macroscopic and Microscopic Aspects: p. 337-376.
2. Van Duin, A.C., S. Dasgupta, F. Lorant, and W.A. Goddard, *ReaxFF: a reactive force field for hydrocarbons.* The Journal of Physical Chemistry A, 2001. **105**(41): p. 9396-9409.
3. Ludwig, J., D.G. Vlachos, A.C. Van Duin, and W.A. Goddard, *Dynamics of the dissociation of hydrogen on stepped platinum surfaces using the ReaxFF reactive force field.* The Journal of Physical Chemistry B, 2006. **110**(9): p. 4274-4282.
4. Chenoweth, K., S. Cheung, A.C. Van Duin, W.A. Goddard, and E.M. Kober, *Simulations on the thermal decomposition of a poly (dimethylsiloxane) polymer using the ReaxFF reactive force field.* Journal Of The American Chemical Society, 2005. **127**(19): p. 7192-7202.
5. Chenoweth, K., A.C. van Duin, and W.A. Goddard, *ReaxFF reactive force field for molecular dynamics simulations of hydrocarbon oxidation.* The Journal of Physical Chemistry A, 2008. **112**(5): p. 1040-1053.
6. Skorpa, R., J.-M. Simon, D. Bedeaux, and S. Kjelstrup, *Equilibrium properties of the reaction H 2 [right left harpoons] 2H by classical molecular dynamics simulations.* Physical Chemistry Chemical Physics, 2014. **16**(3): p. 1227-1237.
7. Skorpa, R., J.M. Simon, D. Bedeaux, and S. Kjelstrup, *The reaction enthalpy of hydrogen dissociation calculated with the Small System Method from simulation of molecular fluctuations.* Physical Chemistry Chemical Physics, 2014. **16**(36): p. 19681-93.
8. Schnell, S.K., X. Liu, J.-M. Simon, A. Bardow, D. Bedeaux, T.J.H. Vlugt, and S. Kjelstrup, *Calculating Thermodynamic Properties from Fluctuations at Small Scales.* The Journal of Physical Chemistry B, 2011. **115**(37): p. 10911-10918.
9. Krüger, P., S.K. Schnell, D. Bedeaux, S. Kjelstrup, T.J. Vlugt, and J.-M. Simon, *Kirkwood–Buff Integrals for Finite Volumes.* The Journal of Physical Chemistry Letters, 2012. **4**(2): p. 235-238.
10. Trinh, T.T., D. Bedeaux, J.M. Simon, and S. Kjelstrup, *Thermodynamic characterization of two layers of CO2 on a graphite surface.* Chemical Physics Letters, 2014. **612**: p. 214-218.

11. Plimpton, S., P. Crozier, and A. Thompson, *LAMMPS-large-scale atomic/molecular massively parallel simulator*. Sandia National Laboratories, 2007. **18**.

12. Cussler, E.L., *Diffusion: mass transfer in fluid systems*. 3 ed. 2009, USA: Cambridge university press.

13. Kjelstrup, S. and D. Bedeaux, *Non-equilibrium thermodynamics of heterogeneous systems*. 2008: World Scientific.

14. Keffer, D., *The Working Man's Guide to Obtaining Self Diffusion Coefficients from Molecular Dynamics Simulations.* Department of Chemical Engineering, University of Tennessee, Knoxville, 2001.

15. Fogler, H.S., *Elements of Chemical Reaction Engineering* 4ed. Prentice Hall International Series in the Physical and Chemical Engineering Sciences. 2006: PTR, Prentice Hall.

16. Atkins, P.W. and J. De Paula, *Atkins' physical chemistry*. 9 ed. 2010: Oxford university press.

17. Helbæk, M. and S. Kjelstrup, *Fysikalsk kjemi*. 2006: Fagbokforl.

18. Krishna, R. and J. Wesselingh, *The Maxwell-Stefan approach to mass transfer.* Chemical Engineering Science, 1997. **52**(6): p. 861-911.

19. Terrell, L., *Hill, An introduction to statistical thermodynamics*. 1 ed. Addison-wesley series in chemistry. 1960: Addison-Wesley.

20. Leach, A.R., *Molecular modelling: principles and applications*. Second ed. 2001: Pearson education.

21. Plimpton, S., *Fast parallel algorithms for short-range molecular dynamics.* Journal of computational physics, 1995. **117**(1): p. 1-19.

22. Tuckerman, M., B.J. Berne, and G.J. Martyna, *Reversible multiple time scale molecular dynamics.* The Journal of chemical physics, 1992. **97**(3): p. 1990-2001.

23. Field, M.J., *A practical introduction to the simulation of molecular systems*. 3 ed. 2007, United Kingdom: Cambridge University Press.

24. Frenkel, D. and B. Smit, *Understanding molecular simulation: from algorithms to applications*. Vol. 1. 2001: Academic press.

25. Simon, J.-M., O.-E. Haas, and S. Kjelstrup, *Adsorption and desorption of H2 on graphite by molecular dynamics simulations.* The Journal of Physical Chemistry C, 2010. **114**(22): p. 10212-10220.

26. Allen, M.P. and D.J. Tildesley, *Computer simulation of liquids*. 1989: Oxford university press.

27. Stillinger, F.H. and T.A. Weber, *Molecular dynamics simulation for chemically reactive substances. Fluorine.* The Journal of chemical physics, 1988. **88**(8): p. 5123-5133.
28. Kohen, D., J.C. Tully, and F.H. Stillinger, *Modeling the interaction of hydrogen with silicon surfaces.* Surface science, 1998. **397**(1): p. 225-236.
29. Diedrich, D.L. and J.B. Anderson, *An Accurate Quantum Monte Carlo Calculation of the Barrier Height for the Reaction.* Science, 1992. **258**(5083): p. 786-788.
30. Diedrich, D.L. and J.B. Anderson, *Exact quantum Monte Carlo calculations of the potential energy surface for the reaction H+ H2→ H2+ H.* The Journal of chemical physics, 1994. **100**(11): p. 8089-8095.
31. Hill, T.L., *Thermodynamics of small systems*. 1963: Courier Corporation.
32. Schnell, S.K., *Molecular Simulations of Zeolites: Heterogeneous Systems at Equilibrium and Non-Equilibrium*. 2013: TU Delft, Delft University of Technology.
33. Schnell, S.K., R. Skorpa, D. Bedeaux, S. Kjelstrup, T.J. Vlugt, and J.-M. Simon, *Partial molar enthalpies and reaction enthalpies from equilibrium molecular dynamics simulation.* The Journal of chemical physics, 2014. **141**(14): p. 144501.
34. Lemmon, E., M. McLinden, and D. Friend, *Thermophysical Properties of Fluid Systems in NIST Chemistry WebBook, NIST Standard Reference Database Number 69, Eds. Linstrom, PJ and Mallard, WG, National Institute of Standards and Technology, Gaithersburg MD, 20899.* webbook. nist. gov (accessed September 1, 2015), 2011.
35. Aylward, G.H. and T.J.V. Findlay, *SI chemical data*. 6 ed. 1973: New York, Wiley.
36. Nicholas, J.B., F.R. Trouw, J.E. Mertz, L.E. Iton, and A.J. Hopfinger, *Molecular dynamics simulation of propane and methane in silicalite.* The Journal of Physical Chemistry, 1993. **97**(16): p. 4149-4163.
37. van Duin, A.C., J.M. Baas, and B. van de Graaf, *Delft molecular mechanics: a new approach to hydrocarbon force fields. Inclusion of a geometry-dependent charge calculation.* Journal of the Chemical Society, Faraday Transactions, 1994. **90**(19): p. 2881-2895.

Appendix A: Calculations of the theoretical self-diffusion coefficients

To calculate the self-diffusion of H_2, Equation(4) was simplified as shown in Equation (1.A). Here, it was assumed that since there was only one species present; $\tilde{M}_1 = \tilde{M}_2$ and $\sigma_1 = \sigma_2$.

$$D_{Self} \frac{1.86 \cdot 10^{-3} T^{3/2} (2/\tilde{M}_1)^{1/2}}{p \sigma_1^2 \Omega} \qquad (1.A)$$

Ω, is as a function of k_bT/ε_{12} and are tabulated in Cussler[12]. Here, ε_{12} is a geometric average of contributions form the two species and k_B is Boltzmann's constant. ε_{12}/k_b of H_2 was found in Cussler[12] as well. The values and units of the different quantities are shown in Table A.1. There were no experimental values for H so the values for He was used instead.

Table A.1. Kinetic gas theory. Values used to calculate the self-diffusion coefficient for H and H_2 using kinetic gas theory

Constant		**Value**	**Value**
D	Diffusion coefficient	-	cm^2/sec
P	Pressure	-	atm
M_i	Molecular weight of H_2	2.02	g/mole
	Molecular weight of H	1.01	g/mole
σ	Diameter of atom spheres of H_2	2.827	Å
	Diameter of atom spheres of He	2.551	Å
ε_{12}/k_b	For H_2	2.827	K
	For He	10.2	K
T	Temperature	-	K
Ω_{H2}	The collision integral for H_2	-	-
Ω_{He}	The collision integral for He	-	-

Appendix B: Uncertainty propagation

To calculate the error propagation, Gauss uncertainty propagation equation is used. The uncertainty of a in a function $y = f(x_1, \ldots, x_p)$, can generally be written as shown in Equation (1.B). Here the s_y and s_x is the standard deviation to the parameters y and x, respectively. The formulas for calculating the uncertainty that is appropriate for this thesis is given below.

$$s_y{}^2 \approx \sum_{i=1}^{p} \left(\frac{\partial f}{\partial x_i} \right)^2 s_{x_i}{}^2 \tag{1.B}$$

The uncertainty for the equilibrium parameter, K_x, is shown in Equation (2.B).

$$s_{K_x}^2 = \left(\frac{\partial K_x}{\partial X_{H_2}} \right)^2 S_{X_2}^2 + \left(\frac{\partial K_x}{\partial X_H} \right)^2 S_X^2 = \left(\frac{2X_H}{X_{H_2}^2} \right)^2 s_{X_{H_2}}^2 + \left(-\frac{X_H^2}{X_{H_2}^2} \right)^2 s_{X_H}^2 \tag{2.B}$$

The uncertainty for ln(y) (where y = K_x or k), is shown in Equation (3.B) and for z^{-1} , (where z = T or h_i)in Equation (4.B).

$$s_{\ln(y)}^2 = \left(\frac{\partial \ln(y)}{\partial y} \right)^2 S_y^2 = \left(\frac{1}{y} \right)^2 S_y^2 \tag{3.B}$$

$$s_{1/z}^2 = \left(\frac{\partial (1/z)}{\partial z} \right)^2 S_z^2 = \left(-\frac{1}{z^2} \right)^2 S_z^2 \tag{4.B}$$

Appendix C: Overview of the state variables used in the simulations

An overview of the state variables used in the simulations and which thermodynamic parameters were directly calculated in LAMMPS is given in Table C.1. As shown, the majority of the thermodynamic parameters for ReaxFF were calculated post modelling.

Table C.1: Overview of the simulation variables

Calculated	Force field	Components	Fixed	Varied	Number of simulations
p	FF	H_2	ρ=3.35 kg/m^3	T= 100-300K.	9
		H_2	Box size = 100^3 Å^3 T =3 00K	N_{H2} = 250-1500	6
		H_2 and H	Box size = 100^3 Å^3 T= 100, K 300K, 500K N_{tot} = 1000	X_{H2} = 0-1	15
MSD	FF	H_2 and H	Box size: 100^3 Å^3 T = 300K N_{tot} = 1000	X_H = 0-1 X_{H2} = 0-1	5
h_{H_2} and h_H	FF	H_2 and H	ρ =5.22 kg/m^3 T = 3639.37 X_{H2} = 0.984	Box size = 28.47^3-98.47^{3}m^3	8
h_{H_2}, h_H and Γ	FF	H_2 and H	ρ =5.22 kg/m^3 X_{H2} = 0.98 Box size = 48.47^{3}Å^3	T = 139-3639	8
H, p	ReaxFF	H_2 and H	ρ =5.22 kg/m^3 Box size = 68.47^{3}Å^3	T = 3639-20796	6

Appendix D: MATLAB codes

```
%-------------------------------------------------------------------
%COUNTING MOLECULES USING THE TRAJECOTRY FILES FROM THE REAXFF
%SIMULATIONS
%-------------------------------------------------------------------
%-------------------------------------------------------------------
%    This code counts the number of molecules in a system with
%    periodic boundary conditions using trajectory files. Additional
%    trajectory %files are created; one for the atoms and one for
%    the molecules.
%
%generated by Nora Meling Eriksen and Thuat Trinh on 2015/05/12
%11:51:42
%-------------------------------------------------------------------
clear all; close all; clc

%start after equilibrium is reached, which is after a 1000 frames
%frame = the positions of a thousand atoms at a given time step
teller1 = 3+1002*1000;. Start at frame 1000
teller2 = 1002+1002*1000; % End of frame 1000

t = -500;
boxsize = 68.469;
filnavn ='T12998.xyz'; % the data file
run = 50; %number of frames


d_max = 1.8;% Å Max length between two atoms in a molecules


for k = 1:run %Defines the number of frames we want
[data(:,1), data(:,2), data(:,3)] =
importfile(filnavn,teller1,teller2);%Imports inn one frame at a
given time step. Importfile was created by a built-in function in
MATLAB

molekyl = 0;
atom = 0;
h2atom = [];
H2atom = [];
H = [];
H2molecule = [];

%One position in the trajectory file is compared with all the
%following positions
for i = 1:size(data,1)
    a = data(i,:); %current position
    z = i+1;
    for p = z:size(data,1)
            b = data(p,:);%the current following position
    if b == a %if the positions are equal, break
        break
    end
        d=sqrt(sum((a-b).^2));%calculates the distance
        if d > boxsize/2   %check PBC for shortest distance
            d2=boxsize;
            for kx=-1:1
                for ky=-1:1
                    for kz=-1:1
                        b=b+[kx,ky,kz]*boxsize;
                        d2=sqrt(sum((a-b).^2));
                        d=min(d2,d);
                    end
                end
            end
        end

      if d <= d_max %if the distance between the two points are
lower or equal to one
        H2atom = [H2atom; data(i,:); data(p,:)]; %collect the
positions to all the atoms that makes molecules
        H2molecule = [H2molecule; data(i,:)]; %collects the
positions to only one of the two atoms in a molecule
        molekyl = molekyl + 1;               %counts a molecule
       break

%if the distance is too large, we have to check if the atom is found
at the boundary of the box since we have periodic boundary
conditions

      end
    end

end

COM =[d_max/2 d_max/2 d_max/2]; %center of mass
Batom = bsxfun(@minus,H2molecule,COM); %Creates a new atom B from
the H2 molecules

%Must create a vector for Hatoms. Compare data with H2atoms
H = data;
 for i = 1:size(H2atom,1)
     a = bsxfun(@eq,data,H2atom(i,:));%finds where the coordinates
are equal
     z = sum(a,2); %sums up the matrix, if the coordinates are equal
the sum is 3
     b = find(z==3);
        if b > 0
        H(b,:)=[0 0 0]; %removes the positons where a molecules atom
is placed
        end
 end

Hatom = [];
c = find(H(:,1)>0);
for j = 1:size(c) %removes the zeros
    Hatom = [Hatom; H(c(j),:)];
end
t = t + 500; %increases the time step
```

```
 h2atom=unique(h2atom);
 molekyl=size(h2atom)/2;

Mol(k) = molekyl(1,1); %stores the number of molecules for each
frame in a vector which is the length of the number of frames.
Atm(k) = 1000-2*molekyl(1,1); %stores the number of atoms for each
frame in a vector which is the length of the number of frames.
teller1 = teller1 + 1002; teller2 = teller2 + 1002; %moves on to
next frame
Time(k) = t; %creates a vector for the time steps
k
end

%-------------------------------------------------------------------
%SCRIPT AND FUNCTIONS TO CALCULATE THE THERMODYNAMIC CORRECTION
%FACTOR USING THE REAXFF TRAJEECTORIES
%-------------------------------------------------------------------

%-------------------------------------------------------------------
%THE SCRIPT
%     This script calculates the thermodynamic correction factor for
%     a mixture of H and H2 using the Small System Method and plots
%     them. In this script is all the initial values defined which is
%     used in the function TDF_Nora. The output of the function is
%     plotted.
%
%generated by Nora Meling Eriksen on 2015/05/12 11:51:42
%-------------------------------------------------------------------
clear all; close all; clc

%The file we are calculating from
filnavn ='T3639.xyz'; %Imports the data file

%Initial values for the counting code
boxsize = 68.48;
d_max = 1.8;      % Maximum distance between two atoms in a molecule
rmin = 0.05;      % Smallest radius in the small system spheres
rmax = 0.4790;    % Largest radius in the small system spheres
numVolumes = 200;% Number of small system spheres
numRadii= 30;     % Number of radii
run = 50;         % Number of time steps
covHB = [];

%Perform SSM in each atom vector
data=
TDF_Nora(rmin,rmax,numVolumes,numRadii,run,filnavn,boxsize,d_max);
R =(data.radius);
L =((((4/3)*pi).*R.^3).^(1/3).*boxsize); %scaling L to the correct
boxsize
L_1 =fliplr((L.').^-1); %makes sure the largest box size is first
sphH =(data.spheresH);
gammaH = var(sphH,1)./mean(sphH); % 1/Gamma
sphB =(data.spheresB);
gammaB = var(sphB,1)./mean(sphB); % 1/Gamma
for g = 1:30
C = cov(sphB(:,g),sphH(:,g));
```

```
covHB = [covHB; C(1,2)];
end
gammaHB = (covHB.')./mean(sphH); %1/Gamma

 figure
plot(L_1,gammaH,'-*',L_1,gammaB,'-o',L_1,gammaHB,'-^')
xlabel('1/L [Å^-^1]');
ylabel('\Gamma^{-1}');
legend('H-H','H_2-H_2','H-H_2','location','best')
box off
legend('boxoff')
save('gammaT3936.mat','gammaH','gammaB','gammaHB')


%-------------------------------------------------------------------
%THE SMALL SYSTEM METHOD FUNCTION
%     This code creates two new trajectories for H and H2 in a
%     mixture of H2 and H. The Small System Method is used to
%     calculate the thermodynamic correction on each trajectory.
%     This code imports the initial variables set in the script
%
%generaded by Bjørn Strøm, Nora Meling Eriksen and Thuat Trinh
%on 2015/05/12 11:51:42
%-------------------------------------------------------------------
function [varargout] =
TDF_Nora(rmin,rmax,numVolumes,numRadii,run,filnavn,boxsize,d_max)

RangeY = 1;

%% Initialize variables
radius =[rmin:0.0042:0.114 0.115:0.028:rmax];
spheresH = zeros(numVolumes*10000,numRadii);
sphere_countsH = zeros(numVolumes,numRadii);
spheresB = zeros(numVolumes*10000,numRadii);
sphere_countsB = zeros(numVolumes,numRadii);
%% Counting code
teller1 = 3+1002*1000;
teller2 = 1002+1002*1000;

for k = 1:run
[data(:,1), data(:,2), data(:,3)] =
importfile(filnavn,teller1,teller2);
atom = 0;
h2atom = [];
H2atom = [];
H = [];
H2molecule = [];

for i = 1:size(data,1)
    a = data(i,:);
    z = i+1;
    for p = z:size(data,1)
            b = data(p,:);
    if b == a
        break
    end
```

```
        d=sqrt(sum((a-b).^2));

        if d > boxsize/2
            d2=boxsize;
            for kx=-1:1
                for ky=-1:1
                    for kz=-1:1
                        b=b+[kx,ky,kz]*boxsize;
                        d2=sqrt(sum((a-b).^2));
                        d=min(d2,d);
                    end
                end
            end
        end

      if d <= d_max
        H2atom = [H2atom; data(i,:); data(p,:)];
        H2molecule = [H2molecule; data(i,:)];
       break
      end
    end

end

COM =[d_max/2 d_max/2 d_max/2];
Batom = bsxfun(@minus,H2molecule,COM);
H = data;
 for i = 1:size(H2atom,1)
     a = bsxfun(@eq,data,H2atom(i,:));
     z = sum(a,2);
     b = find(z==3);
        if b > 0
        H(b,:)=[0 0 0];
        end
 end

Hatom = [];
c = find(H(:,1)>0);
for j = 1:size(c)
    Hatom = [Hatom; H(c(j),:)];
end

atomCoordinatesH = Hatom./boxsize;
atomCoordinatesB = Batom./boxsize;

    for l = 1:numVolumes
            [sphere_countsH(l,:)] =
PBC_Nora(radius,atomCoordinatesH);
            [sphere_countsB(l,:)] =
PBC_Nora(radius,atomCoordinatesB);
    end

    spheresH(1+(k-1)*numVolumes:k*numVolumes,:) = sphere_countsH;
    spheresB(1+(k-1)*numVolumes:k*numVolumes,:) = sphere_countsB;

teller1 = teller1 + 1002;
```

```
teller2 = teller2 + 1002;
k
end

spheresH(k*numVolumes+1:end,:) = [];
spheresB(k*numVolumes+1:end,:) = [];

%OUTPUTS IN SAME VARIABLE STRUCTURE
varargout{1}.spheresH = fliplr(spheresH);
varargout{1}.spheresB = fliplr(spheresB);
varargout{1}.radius = radius;
varargout{1}.RangeY = RangeY;

end

%-------------------------------------------------------------------
%PBC_NORA takes in a (1 x a) vector of radii, and an (m x n) matrix
%   of atom coordinates. The output is a (1 x a) vector where each
%   element is the number of atoms located within a spherical
%   selection with the corresponding radius given by the provided
%   input vector. The selections are random, for each time the
%   function is called, but have the same center for each radius
%   within the same call. This is done for computational efficiency
%   because it allows us to shrink the selection from largest to
%   smallest radius.
%
%   m = no. of atoms
%   n = 3 (x, y, z) The coordinates are scaled between 0 and 1 to
%   represent a fraction of the simulation box size.
%
% generated by Bjørn Strøm on 2015/05/12 11:51:42
%-------------------------------------------------------------------

function [sphere_count] = PBC_Nora(radius,atom_coordinates)

num_radii = length(radius);
radius = fliplr(radius); % the radius vector is reversed to allow..
sphere_c = rand(1,3); % ..the selections to shrink in size
box_c = [0.5,0.5,0.5]; % simulation box center position
trans_vec = box_c - sphere_c; % translation vector for PBC
sphere_list = bsxfun(@plus,atomCoordinates,trans_vec); % Translates…
sphere_count = zeros(numRadii,1); % … atom Coordinates with
trans_vec.

%% Wrap the spherical selection for periodic boundary conditions
if trans_vec(1) > 0
    x_check = bsxfun(@gt,sphere_list(:,1),1);
    sphere_list(:,1) = sphere_list(:,1) - x_check;
else
    x_check = bsxfun(@lt,sphere_list(:,1),0);
    sphere_list(:,1) = sphere_list(:,1) + x_check;
end

if trans_vec(2) > 0
    y_check = bsxfun(@gt,sphere_list(:,2),1);
    sphere_list(:,2) = sphere_list(:,2) - y_check;
```

```
else
    y_check = bsxfun(@lt,sphere_list(:,2),0);
    sphere_list(:,2) = sphere_list(:,2) + y_check;
end

if trans_vec(3) > 0
    z_check = bsxfun(@gt,sphere_list(:,3),1);
    sphere_list(:,3) = sphere_list(:,3) - z_check;
else
    z_check = bsxfun(@lt,sphere_list(:,3),0);
    sphere_list(:,3) = sphere_list(:,3) + z_check;
end

% Make a spherical selection for each radius
for i = 1:numRadii
    sphere_select = ((sphere_list(:,1) - box_c(1)).^2 +
(sphere_list(:,2) - box_c(2)).^2 + (sphere_list(:,3) - box_c(3)).^2
) <= radius(i)^2;
    sphere_count(i) = sum(sphere_select);
    sphere_list = reshape(sphere_list(repmat(sphere_select,[1,3])),
[sphere_count(i),3]);
end
end
```

Appendix E: ReaxFF input in LAMMPS

```
#hydrogen with ReaxFF potential at 3639K
boundary p p p
restart 1000000 restart
#Simulation Units
units real
atom_style charge
#Reads configuration from file
#read_restart restart.last
read_data init.data
#Mass relative mass of atoms
mass 1 1.08000

pair_style     reax/c lmp_control
pair_coeff      * * ffield.reax.cho H
thermo_style   multi
neigh_modify delay 0 every 1 check yes

#Applies or "fixes" NVT MD
velocity        all create 100.0 234324324 dist gaussian mom yes rot yes
###set NVT
variable T equal 3639

fix                  1 all nve
fix             2 all qeq/reax 1 0.0 10.0 1e-6 param.qeq
fix             3 all temp/berendsen $T $T 100

##compute temp over x axe
```

```
dump            1 all xyz 500 h2_trj.xyz
dump_modify 1 element H
#Dumps output files and thermodynamic properties
thermo_style custom step temp press pe enthalpy
thermo          500
#Timestep is 1 fs (0.001 ps)
timestep 0.1
#dump 2 all atom 30 dump.reax.test
#Number of time steps
run     1000000
```

Symbol List

Table 1: Latin symbols

Symbol	Dimension	Explanation
J_i	/s	Total flux
j_i	m^2/s	Flux per area
c	mol/L	Concentration
a	m^2	Cross sectional area
D	m^2/s	Ficks diffusivity
z	m	Distance
t	s	Time
D_{self}	m^2/s	Self-diffusion
d	-	Dimensionality
$\mathbf{r}(t)$	Å	Molecular position
b_o	-	Intercept
T	K	Temperature
p	bar	Pressure
$\tilde{M}_i$	g/mol	Molecular weight of species i
E_a	kJ/mol	Activation energy
ΔH_f	kJ/mol	Average bond enthalpy
k_r	1/fs	Rate constant
A	/s	Frequency factor
R	J/mol K	Universal gas constant
[A]	-	Change in concentration
H	J	Enthalpy
V	$Å^3$	Volume
U	J	Internal energy
h_i	kJ/mol	Partial molar enthalpy of species i
q	kJ	Heat
n_i	mol	Number of moles of species i
C	J/K	Heat capacity
$C_{p.i}$		Molar heat capacity of species i
$\Delta_r H$	J/mol	Reaction enthalpy

Table 1: Latin symbols continued

Symbol	Dimension	Explanation
Đ	m^2/s	Maxwell-Stefan diffusivity
m_i	kg	Mass of species i
f	N	force
p_i	kg	Momentum
$V(\mathbf{r}_i)_i$	J	Potential
$\hat{H}$	-	Hamiltonian
K_{th}	-	Thermodynamic equilibrium constant
K_x	-	Dissociation constant
X_i	-	Mole fraction of species i
N_i	-	Number of particles of species i
B	-	Thermodynamic property
M	-	Number of time steps
L_t	Å	Total system length
L	Å	Small system length
r_n	Å	Small system radius
r*	-	Small system radius in reduced units
r_{ij}	Å	Separation distance
k_B	m^2kg/s^2K	Boltzmann constant
F_2	J	force functions for the pair-wise interaction
F_3	J	force functions for a three-body interaction

Table 2: Greek symbols

Symbol	Dimension	Explanation
σ	Å	Collision diameter
Ω	-	Collision integral
ε_{12}	-	A geometric average of contribution from two species
γ_i	-	Activity constant
Γ_i	-	Thermodynamic correction factor
μ_i	J/mol	Chemical potential
ρ	kg/m^3	Density
π	-	Pi

Table 3: Mathematical symbols, superscripts, subscripts

Symbol	**Explanation**
0	Subscript meaning initial value
Cov()	Covariance
Var()	Variance
Mean()	Arithmetic average
$\langle\ \rangle$	Time average
$\equiv$	Defined by
d	Differential
∂	Partial deviated
$\ddot{a}$	Second deviation
N	Superscript meaning a vector of N dimensions
s	Standard deviation
$\mathbf{a}$	Vector
Δ	Change in a quantity of variable

Table 4: Abbreviations

Symbol	**Explanation**
SSM	Small System Method
MSD	Mean square displacement
TCF	Thermodynamic correction factor
MD	Molecular dynamics
FF	Classical force field
TBP	Three-body potential
DMM	Delft Molecular mechanics
STD	Standard deviation
KGT	Kinetic gas theory

Table of Figures

Figure 2.1: The movements for hydrogen molecule and atom. 6

Figure 3.1: Illustration of the small systems embedded in a reservoir.................................... 16

Figure 4.1: A snap shot of the system at density, ρ=1.67kg/m^3... 20

Figure 5.1: $p(T)$ with the FF. 26

Figure 5.2: $p(N_{H_2})$with the FF. 27

Figure 5.3: $p(X_{H_2})$with the FF. 27

Figure 5.4: MSD(t) with the FF. 28

Figure 5.5: $h_i^{-1}(r^{*-1})$ at different box sizes with the FF. 30

Figure 5.6: $h_i^{-1}(L)$ at different temperature with the FF. 30

Figure 5.7: $h_{i,\infty(}T)$ with the FF. 31

Figure 5.8: Γ_{HH}^{-1} (L^{-1}) at different temperatures with the FF. 33

Figure 5.9: MSD(t) with the ReaxFF. 35

Figure 5.10 $D_{self,i}(T)$ with the ReaxFF. 35

Figure 5.11: $h_i(t)$ with ReaxFF. 37

Figure 5.12: $h_i(T)$ with ReaxFF. 37

Figure 5.13: $\Gamma_{ij}^{-1}(L^{-1})$ with the ReaxFF.. 39

Figure 5.14: The correction factor at the thermodynamic limit with RreaxFF. 40

Figure 5.15: Finding the reaction constant for ReaxFF. 41

Figure 5.16: Finding the activation energy for ReaxFF. 42

Figure 5.17 Dissociation of H_2. 43

Figure 5.18: Finding the reaction enthalpy for ReaxFF. 44

Table of Tables

Table 4.1: Classical force field parameters 22

Table 4.2: Three-body potential parameters used by Skorpa *et al* 23

Table 5.1: Self-diffusion coefficients ($D_{self,i}$) for H and H_2 with the FF 29

Table 5.2: The molar heat capacity ($C_{p,i}$) of H and H_2 calculated with FF. 31

Table 5.3: The thermodynamic correction factor at the thermodynamic limit. 33

Table 5.4: Data collected from ReaxFF simulations at different temperatures. 34

Table 5.5: The heat capacity of H and H_2 with the ReaxFF. 38

Table 5.6: The thermodynamic correction factor at the thermodynamic limit ($\Gamma_{ij,\infty}^{-1}$) 39

Table 5.7: The reaction constant (k_r) for the ReaxFF. 42

Table 5.8: The activation energy (E_a) for ReaxFF. 43

Table 5.9: The reaction enthalpy ($\Delta_r H$) for ReaxFF. 44

Table A.1. Kinetic gas theory. 2

Table C.1: Overview of the simulation variables 6

Table 1: Latin symbols 18

Table 2: Greek symbols 20

Table 3: Mathematical symbols, superscripts, subscripts 21

Table 4: Abbreviations 22